Chapter 2

Monoelectron Oscillator

A single electron may be confined indefinitely for study in a Penning trap [92, 11], which is a combination of a strong uniform magnetic field and a quadrupole electrostatic potential [73]. The trap is typically operated at cryogenic temperatures and vacuums. In fact, a vacuum of 5×10^{-17} torr has been deduced using trapped antiprotons [40] in a very similar apparatus. Because of the sensitivity and the long time of confinement, precision measurements are possible that were not feasible using atomic beam techniques. The trap parameters have been controlled in this work in such a way as to increase the sensitivity to the point where the details of the various lineshapes can be exploited for new types of measurements.

In order to detect the signal from a single electron, the apparatus must be extremely stable, homogeneous, and sensitive. These characteristics must hold true for the different subsystems such as the magnetic field, the DC trapping potential, the cryostat, the RF detection system, and the microwave source. In this chapter, we discuss in turn the requirements for each of the systems. But first, we review the motions of a particle confined in a Penning trap.

2.1 Three Oscillators

The classical motions of a particle in a Penning trap are at first glance just three independent simple harmonic oscillators. Closer inspection shows that these oscillators are slightly anharmonic, and in fact are coupled to one another. These anharmonicities and couplings are small and can be measured. In some cases they can be controlled and used to advantage. The oscillators can be driven by thermal noise, or by an external, coherent drive which may be resonant, at a sideband frequency, or parametric. The motions are well understood [11], and are reviewed here only briefly. The three oscillators are shown in Fig. 2.1. The spin of the particle, however, is intrinsically quantum mechanical; and the cyclotron motion at liquid helium temperatures is also quantum mechanical. In fact, it is of interest to study the quantum to classical transition in this motion. This will be discussed in the chapter on the relativistic anharmonic cyclotron oscillator.

An electron of charge $-e$ and mass m in a uniform magnetic field $\mathbf{B}$ moves in a circle with a frequency, ν_c and angular frequency, ω_c given by

$$2\pi\nu_c = \omega_c = \frac{eB}{\gamma mc}. \tag{2.1}$$

Here γ is the familiar relativistic factor, $\gamma = 1/\sqrt{1-(\frac{v}{c})^2}$ The cyclotron radius is

$$r_c = \sqrt{\frac{2E_c}{m\omega_c^2}}, \tag{2.2}$$

where E_c is the energy of the motion. For the largest excitation, we observe $E_c = 16.2\text{eV}$ and $r_c = 2.6 \times 10^{-4}\text{cm}$. This cyclotron motion is typically at a high microwave frequency of about 150 GHz, with a wavelength of 2 mm. The motion is brought to thermal equilibrium with the 4 K environment by synchrotron radiation. The free space damping rate for this spontaneous emission is given by

$$\gamma_c = \frac{4r_0\omega_c^2}{3c} \tag{2.3}$$

where $r_0 \simeq 2.8 \times 10^{-13}$ cm is the classical electron radius and c is the speed of light. At B= 5.3 Tesla the cyclotron frequency $\nu_c = 148$ GHz and $\gamma_c^{-1} = 10^{-1}$ sec. This

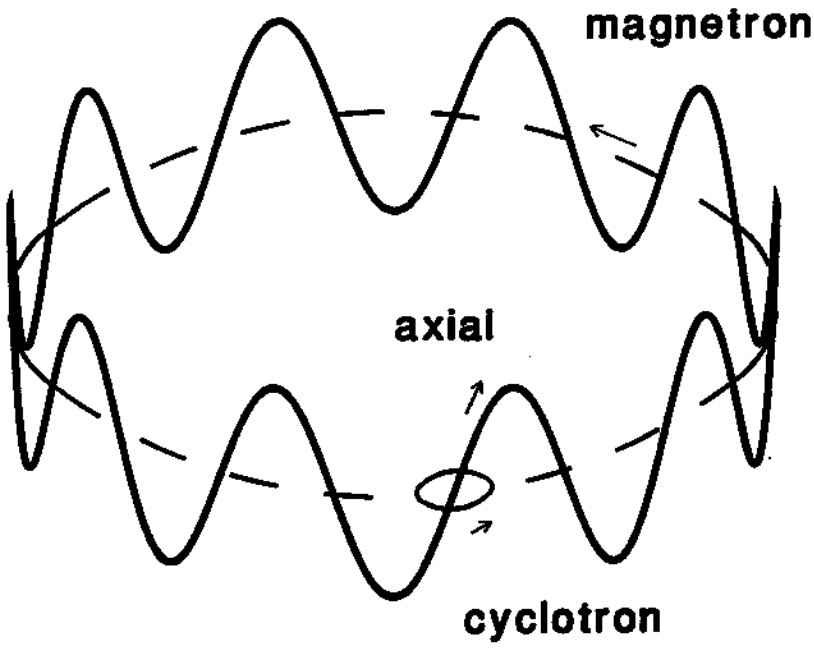

Figure 2.1: The three orthogonal classical motions of a particle in a Penning trap (not to scale). The cyclotron motion is at 148 GHz; the axial motion is at 63.4 MHz; and the magnetron motion is at 13.6 kHz.

spontaneous emission rate can be either enhanced or inhibited by the environment [38]. The cyclotron oscillation is the motion we wish to study.

An electrostatic quadrupole potential is superimposed on the uniform magnetic field to confine the particle axially. The electron moves up and down in the potential, which along the vertical axis is simply a harmonic well. The potential is of the form

$$V(\rho, z) = V_0 \frac{z^2 - \rho^2/2}{2d^2} \tag{2.4}$$

where V_0 is the voltage applied between the ring and endcaps, and d is a characteristic trap dimension. The angular frequency of the axial motion (in an ideal harmonic potential) is given by

$$\omega_z^2 = \frac{eV_0}{md^2}. \tag{2.5}$$

Typically, the trapping potential is $V_0 = 10.193$ Volts, which gives an axial frequency $\nu_z = 63.7$ MHz. Damping of this axial motion is dominated not by radiative damping ($\gamma_{z,rad}^{-1} \simeq 10^6$ sec) but by coupling to the detection circuit (typically, $\gamma_z^{-1} \simeq 1.3 \times 10^{-2}$ sec), which will be described later. To learn about the cyclotron motion, we detect the axial motion directly, taking advantage of small couplings between these motions.

A third oscillator arises from the combination of perpendicular components of the electric and magnetic field. These fields act as a velocity filter, allowing only the velocity $\mathbf{v} = c\mathbf{E} \times \mathbf{B}/B^2$. The motion, called the magnetron motion, has a constant frequency

$$\nu_m = \frac{\nu_z^2}{2\nu_c'}. \tag{2.6}$$

This results in a slight reduction of the observed cyclotron frequency, ν_c', by the magnetron frequency: $\nu_c' = \nu_c - \nu_m$. For $\nu_c = 147.6$ GHz and $\nu_z = 63.374$ MHz, $\nu_m = 13.6$ kHz. The magnetron motion is metastable. The radius of the magnetron orbit actually increases as this motion is damped, but fortunately the radiative damping time is extremely long. The radius of the magnetron orbit can be reduced

by applying appropriate sideband drive fields [91], and thereby localizing the electron near the center of the trap. Near the center of the trap, deviations from an ideal electrostatic potential and homogeneous magnetic field will be less important because the particle will sample only a small region.

The trap unavoidably has misalignments and imperfections which distort the quadrupole potential. Fortunately, it can be shown that the cyclotron frequency that one would measure without the electrodes, ω_c, can be related to the eigenfrequencies that one measures in an imperfect trap through an invariance theorem [11],

$$\omega_c^2 = \bar{\omega}_c^2 + \bar{\omega}_z^2 + \bar{\omega}_m^2 \tag{2.7}$$

There is a clear hierarchy among the measured eigenfrequencies of the three oscillators:

$$\bar{\omega}_c \gg \bar{\omega}_z \gg \bar{\omega}_m. \tag{2.8}$$

Under our typical conditions, $\bar{\nu}_c = 147.6$ GHz, $\bar{\nu}_z = 63.374$ MHz, and $\bar{\nu}_m = 13.6$ kHz.

2.2 Magnetic Field

In order to make a precision measurement of the electron cyclotron frequency, the magnetic field environment must be both stable and homogeneous. Since the cyclotron frequency is directly proportional to the magnetic field, any temporal variation of the field will translate to a temporal variation of the frequency, and thus will cause a line broadening. Furthermore, since the electron oscillates over a finite extent in the trap, it will sample different magnetic fields if there are any inhomogeneities. This results in a not well-defined frequency, and again to another line broadening. Therefore, it is paramount for a precision measurement to create a stable and homogeneous magnetic field. Furthermore, the value of the magnetic field is chosen to be as large as possible for two reasons. First, the fractional error

in the cyclotron frequency due to field fluctuations is equal to the ratio of the field fluctuation to the overall field strength. Therefore, the larger the field, the smaller the fractional frequency error. Second, the cyclotron quantum level spacing (Landau levels), which is proportional to the field strength, must be large enough so that the Boltzmann distribution among the levels is mostly in the ground state. (Typically, the electron is in the ground state 82 percent of the time.)

The magnetic field for the Penning trap is produced by a superconducting magnet designed for high resolution measurements. Over 25 miles of monofilament NbTi wire form the solenoid which produces a strong homogeneous magnetic field (typically 5 Tesla). The liquid helium reservoir for the solenoid is pressure regulated (the shift due to pressure is measured to be 2 ppb/Torr). The bore opening is about 100 millimeters in diameter, allowing placement of the Penning trap in the high field region. The magnet has two main solenoids, configured in such a way as to permit minimization of the second order field gradient in the vertical direction. Cylindrical symmetry of the construction substantially reduces the azimuthal gradients. There is a series of small superconducting shim coils with different Legendre polynomial symmetries to tune out any residual gradients. There are a few non-superconducting coils to fine tune the field or to create a deliberate gradient. The homogeneity is initially checked with a standard NMR probe using acetone. The field can be adjusted to give an NMR proton linewidth of 2 Hz out of 250 MHz using a 1 centimeter diameter probe sample. The linear gradient in the vertical direction is initially minimized by adjusting the shim coils so that the signal from a small probe does not vary as it is moved up and down in the field. This gradient is later checked *in situ* by measuring the cyclotron frequency of a cloud of electrons which is offset at different vertical positions.

2.2.1 Shielding Using Flux Conservation

In order to make a precision measurement of the cyclotron frequency of an electron to one ppb (the precision needed to distinguish a spin flip of the electron), the field must be stable at that level over the time scale of the measurement. There are fluctuations in the ambient magnetic field due to a variety of sources, such as day/night fluctuations in the earth's magnetic field, solar storms, and disturbances from the MBTA subway line near the laboratory. The measured fluctuations at night are about 0.1- 0.6 mG, and during the day 3 mG is typical.

The desired stability of one ppb of a 6 Tesla field (0.06 mG) is much smaller than these fluctuations. Fortunately, fluctuations faster than 1 Hz are shielded by eddy currents in the metal structures in the magnet bore. The superconducting solenoid is also designed to compensate for uniform magnetic field variations by exploiting flux conservation [44]. A superconducting loop will respond to an ambient external field change ΔB_e by creating a response field ΔB_r such that the flux is conserved,

$$\Delta\Phi = \int dA(\Delta B_e + \Delta B_r) = 0. \tag{2.9}$$

The value of the response field at the origin, $B_r(0)$, is related to the response flux by the geometry of the coil. This geometry can be chosen so that the total field change at the origin is zero,

$$\Delta B(0) = B_e + B_r(0) = 0. \tag{2.10}$$

Here, we assume that the external field is uniform ($B_e(0) = B_e$). The particles are localized near the origin, and so will see a stable field. The particular superconducting magnet used in these experiments shields the ambient field fluctuations by a factor of 175. Changes in the total field due to fluctuations in the transverse directions must be added in quadrature to the 6 Tesla main field, and thus are much less important. One further advantage of this shielding method is that it is entirely passive.

2.2.2 Quadratic Gradient

To avoid motional broadening of the cyclotron resonance lineshape, the magnetic field must also be homogeneous. In the axial direction, the linear gradient gives a broadening of the line without a shift; the quadratic gradient gives both a broadening and a shift. Azimuthal gradients can also be important, especially in precision mass comparisons of heavier species where the orbits can have large radii. In conjunction with minimizing the spatial magnetic field gradients, minimizing the spatial extent of the electron orbits, such as the axial excursion or the magnetron orbit radius, is also desirable.

The quadratic gradient, often called a magnetic bottle, is of particular importance because in some ways it mimicks the relativistic detection coupling between the cyclotron and axial oscillators [39, 11]. Special relativity causes a shift in the axial frequency whenever there is a shift in the cyclotron frequency. To see this, recall from Eq. 2.1 that [74]

$$2\pi\nu_c = \omega_c = \frac{eB}{\gamma mc} \tag{2.11}$$

and

$$2\pi\nu_z = \omega_z = \sqrt{\frac{eV}{\gamma md^2}}, \tag{2.12}$$

where γ is the familiar relativistic factor,

$$\gamma = \frac{1}{\sqrt{1-(\frac{v}{c})^2}} = 1 + \frac{K}{mc^2}, \tag{2.13}$$

which can be expressed in terms of either the velocity,v, or the kinetic energy, K. Therefore,

$$\frac{\Delta\omega_z}{\omega_z} = \frac{1}{2}\frac{\Delta\omega_c}{\omega_c} \tag{2.14}$$

Thus, a shift in the cyclotron frequency can produce an observable shift in the axial frequency. This coupling between the axial and cyclotron motions can also be

formed by means of a magnetic bottle which is a second order field gradient. The relativistic coupling produces the same shifts to the axial frequency as a magnetic bottle of strength -4.7 G/cm^2. It is important to note that the "relativistic bottle", while providing a detection coupling, does not distort the magnetic field, and thus motion through it does not broaden the cyclotron line.

A magnetic bottle is a quadratic distortion of the field of the form:

$$\mathbf{\Delta B} = B_2[(z^2 - \rho^2/2)\hat{\mathbf{B}} - (\hat{\mathbf{B}} \cdot \mathbf{z})\rho]. \tag{2.15}$$

A magnetic moment, $\vec{\mu}$, adds a term to the Hamiltonian given by

$$\Delta H = -\vec{\mu} \cdot \mathbf{\Delta B} = -\mu B_2 z^2. \tag{2.16}$$

which has a form of an effective spring constant in the axial direction. For $B_2 < 0$, it is a confining potential which is why this magnetic gradient is called a magnetic bottle.

The interactions between the different degrees of motion through the relativistic coupling and through the external magnetic bottle can be summarized in a matrix [11](note typographical error of the cyclotron to spin coupling in Eq. 10.21 of the reference), $M = M_B + M_R$, that relates the fractional shift in the cyclotron, axial, magnetron, and spin frequencies to excitations in the different energies,

$$\begin{pmatrix} \frac{\Delta\omega_c}{\omega_c} \\ \frac{\Delta\omega_z}{\omega_z} \\ \frac{\Delta\omega_m}{\omega_m} \\ \frac{\Delta\omega_s}{\omega_s} \end{pmatrix} = M \begin{pmatrix} E_c \\ E_z \\ E_m \end{pmatrix} \tag{2.17}$$

where

$$M_R = -\frac{1}{mc^2} \begin{pmatrix} 1 & \frac{1}{2} & -(\omega_z/\omega_{c'})^2 \\ \frac{1}{2} & \frac{3}{8} & -\frac{1}{4}(\omega_z/\omega_{c'})^2 \\ -(\omega_z/\omega_{c'})^2 & -\frac{1}{4}(\omega_z/\omega_{c'})^2 & \frac{1}{4}(\omega_z/\omega_{c'})^4 \\ 1 & \frac{1}{2} & -(\omega_z/\omega_{c'})^2 \end{pmatrix} \tag{2.18}$$

and

$$M_B = \frac{\Delta\tilde{\omega}_z}{\omega_z}\frac{1}{\hbar\omega_c'}\begin{pmatrix} -(\omega_z/\omega_{c'})^2 & 1 & 2 \\ 1 & 0 & -1 \\ 2 & -1 & -2 \\ -(\omega_z/\omega_{c'})^2 & 1 & 2 \end{pmatrix} \tag{2.19}$$

where

$$\frac{\Delta\tilde{\omega}_z}{\omega_z}\frac{1}{\hbar\omega_c'} = \frac{1}{2m\omega_m\omega_c'}\frac{B_2}{|B|}. \tag{2.20}$$

Thus, we can see from this matrix that the anharmonicity strength of the cyclotron motion is primarily due to the relativistic coupling. Explicitly,

$$\frac{\Delta\omega_c}{\omega_c} = [-\frac{1}{mc^2} + -(\omega_z/\omega_{c'})^2\frac{\Delta\tilde{\omega}_z}{\omega_z}\frac{1}{\hbar\omega_c'}] \times \mathrm{E_c} \tag{2.21}$$

The contribution from the external bottle is small. For comparison, a deliberate external magnetic bottle would have to be very large, ($\frac{B_2}{|B|} = \left[\frac{\omega_c}{c}\right]^2$, which is about $10^3/\mathrm{cm}^2$), to produce an equivalent cyclotron frequency shift. On the other hand, the detection strength (axial frequency shift) has comparable contributions from the relativistic and external magnetic bottle couplings. The detected axial frequency shift is given by the matrix as,

$$\frac{\Delta\omega_z}{\omega_z} = [-\frac{1}{2mc^2} + \frac{\Delta\tilde{\omega}_z}{\omega_z}\frac{1}{\hbar\omega_c'}] \times \mathrm{E_c} \tag{2.22}$$

This relativistic axial coupling can be mimicked by a quadratic gradient $\frac{B_2}{|B|} = -\frac{1}{2}\left(\frac{\omega_z}{c}\right)^2$, which is about $-10^{-4}/\mathrm{cm}^2$. Thus, the relativistic coupling between the cyclotron energy and the cyclotron frequency (anharmonicity) is extremely strong, whereas the relativistic coupling between the cyclotron energy and the axial frequency (detection) is weak.

The cyclotron frequency is also shifted by the axial energy, $\mathrm{E_z}$. This is given by

$$\frac{\Delta\omega_c}{\omega_c} = [-\frac{1}{2mc^2} + \frac{\Delta\tilde{\omega}_z}{\omega_z}\frac{1}{\hbar\omega_c'}] \times \mathrm{E_z} \tag{2.23}$$

This implies that noise from the detector will cause a broadening of the cyclotron frequency. For example, a thermal 4.2 K distribution in the axial motion will cause

a broadening of the cyclotron line by approximately one third the spacing between the levels, δ. This back coupling can be eliminated by choosing an external magnetic bottle to cancel the relativistic bottle, $\frac{B_2}{|B|} = +\frac{1}{2}\left(\frac{\omega_z}{c}\right)^2$. However, this also eliminates the detection coupling. This can be expressed as,

$$\left[\frac{d\left(\frac{\Delta\omega_c}{\omega_c}\right)}{dE_z}\right] = \left[\frac{d\left(\frac{\Delta\omega_z}{\omega_z}\right)}{dE_c}\right]. \tag{2.24}$$

A scheme to reverse and reduce the bottle has been tried [68, 69, 39]. This has the advantage of providing a sharp feature in the lineshape on the lower frequency side, thereby allowing a more precise determination of the $n = 0$ to $n = 1$ transition frequency. Bottles of strength 10G/cm^2 and 30G/cm^2 were reported [68, 69, 26]. This is much smaller than the 150G/cm^2 magnetic bottle used in the latest determination of the electron g factor [85]. The bottle of strength 10G/cm^2 reverses the Boltzmann tail of the cyclotron lineshape, but keeps the same magnitude. This was sensitive enough to detect spin flips of the electron.

The coupling between the cyclotron and axial motions can be measured directly [39]. To do this, the cyclotron drive is swept by a calibrated amount. This will excite the relativistic anharmonic cyclotron oscillator and shift the frequency by a large amount according to the relativistically dominated cyclotron-cyclotron coupling. Through the (relativistic and external magnetic bottle) cyclotron-axial coupling the axial frequency will shift by a relatively small amount. The ratio of these shifts will then give the size of the coupling. We measure in the hyperbolic trap a coupling of $\eta = 1.41$, where

$$\eta = \frac{\Delta\omega_c/\omega_c}{\Delta\omega_z/\omega_z} = \frac{2}{1 + \frac{2c^2}{\omega_z^2}(B_2/B)}. \tag{2.25}$$

Here, B_2/B is the actual magnetic bottle (that is, $\eta = 2$ for no magnetic bottle). This external magnetic bottle has a strength $1.9\ \text{G/cm}^2$, which corresponds to -0.4 of a relativistic bottle. The ratio, η, can be tuned by this method to within 0.5 percent of 2 [39].

2.2.3 Gradient Measurements with Electrons

The magnetic gradients along the vertical direction were measured directly by observing the shift in the cyclotron frequency of a cloud of electrons as they were shifted up and down [36]. This is similar to the previous spatial measurements using a small acetone NMR probe. However, the residual magnetism of the probe and the trap electrodes make it necessary to make more precise measurements with electrons *in situ*. The electron cloud is moved up and down in the trap by adding an asymmetric potential, V_A, across the endcap electrodes. This adds to the quadrupole potential

$$V(r) = \frac{1}{2} V_A \sum_{\substack{k=1 \\ odd}}^{\infty} c_k \left(\frac{r}{d}\right)^k P_k(cos\theta), \tag{2.26}$$

where d and z_0 are characteristic trap dimensions as described in the section on the quadrupole potential. The product, $c_1 c_3$ can be measured from the shift in the axial frequency

$$\frac{\Delta\omega_z}{\omega_z} = -\frac{3}{4}\left(\frac{d}{z_0}\right)\frac{c_1 c_3}{(1+C_2)^2}\left(\frac{V_A}{V_0}\right)^2 \tag{2.27}$$

where the measured $c_1 c_3 = 0.24(1)$ agrees with the calculated $c_1 = 0.784$, $c_3 = 0.320$, and $C_2 = 0.128$ (in the cylindrical trap). This gives for an axial displacement

$$\frac{z_e}{z_0} = -\frac{1}{2}\left(\frac{d}{z_0}\right)^2\left(\frac{V_A}{V_0}\right)c_1. \tag{2.28}$$

Using $V_0 = 10.198$ Volts yields

$$z_e = 0.126\left(\frac{\text{mm}}{\text{Volt}}\right)V_A. \tag{2.29}$$

We thus can conveniently move the electrons to a new equilibrium position, z_e, by adding the additional asymmetric potential.

The magnetic field (from the cyclotron frequency) is then mapped out as a function of vertical position for different magnetic gradient shim settings. The maps are parabolic. The curvature is a measure of the quadratic gradient; and the minima are determined by the linear gradient. Fig. 2.2 shows a family of measurements in

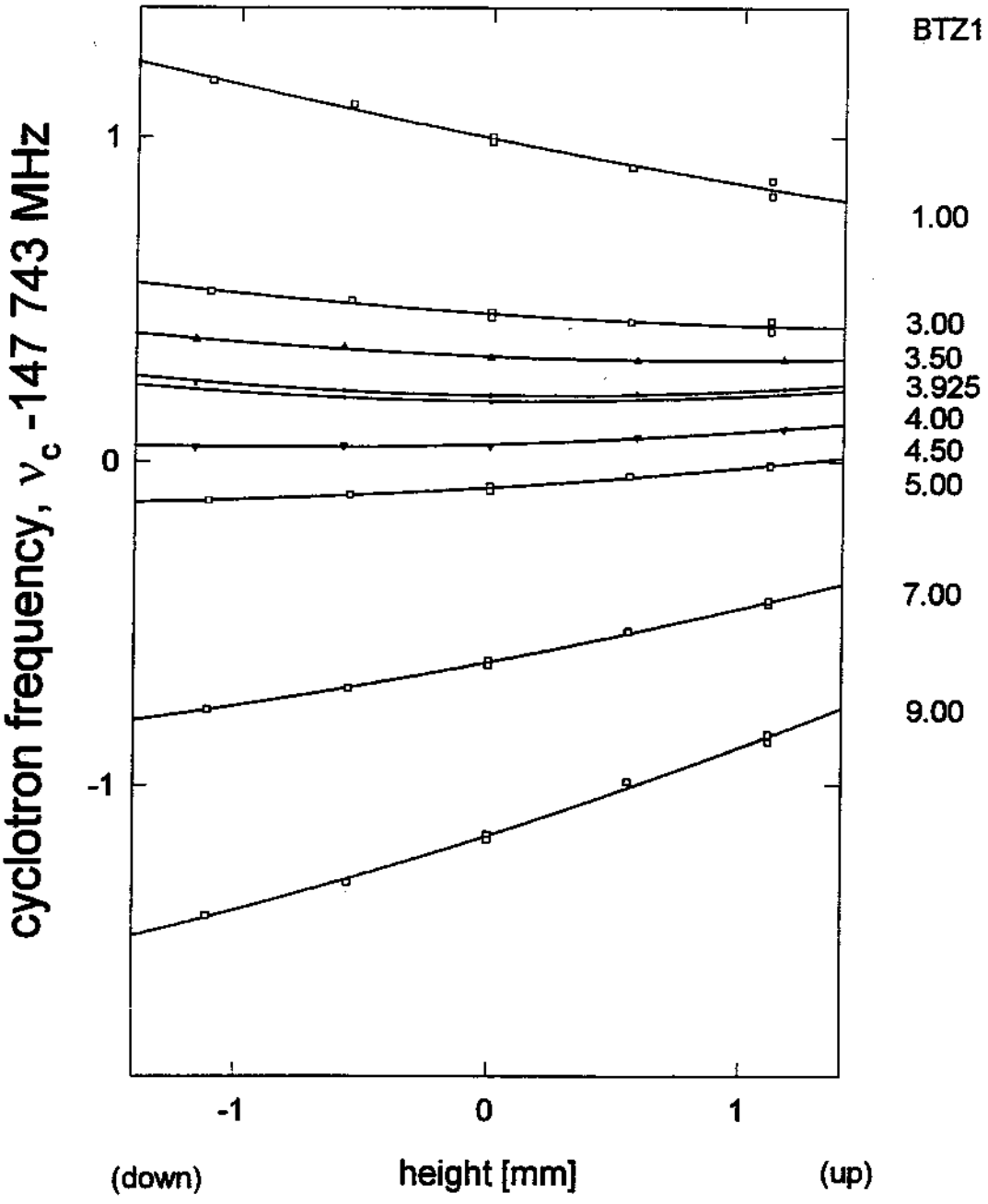

Figure 2.2: The cyclotron frequency shifts as electrons are displaced up and down in the trap. Curves correspond to different gradient shim settings. This maps out the magnetic field in the trap.

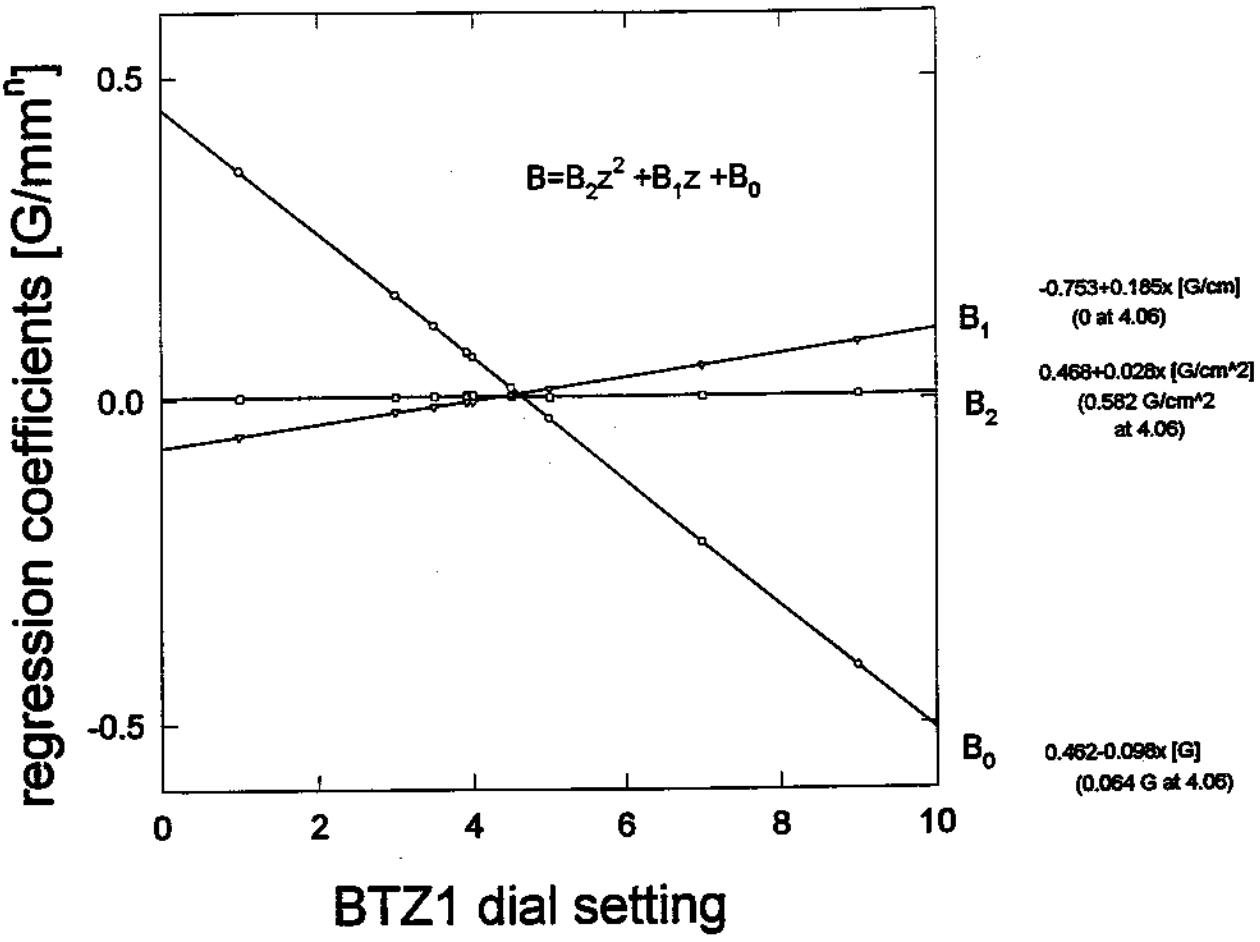

Figure 2.3: Regression coefficients giving the linear and quadratic gradient strengths represented in Fig. 2.2 determine the shim setting (4.06) (for magnet NCC0051) where the linear gradient (B_1) is minimized. The quadratic gradient (B_2) is 0.58 G/cm^2 at this setting.

the cylindrical trap of the cyclotron frequency, ν_c, as z_e is changed. These curves are fit to quadratics, with the linear and quadratic gradients deduced from the regression coefficients. As shown in Fig. 2.3, a shim setting of 4.06 nulls out the linear gradient. This leaves a quadratic gradient of 0.582 G/cm^2, which is -0.12 of its relativistic counterpart.

The quadratic gradient seen by the electron in the trap may come from gradients in the main solenoid coils, the superconducting shim coils, the normal shim coils, or magnetic distortions associated with the trap itself. While each contribution to the quadratic gradient is separately designed to be minimized, the centers of each contribution do not necessarily correspond to the same position. Of course, the *in situ* measurement with the electron cloud yields the net gradient which is of interest. One such magnetic distortion that was designed to be minimized is the contribution of the paramagnetic materials used in the Penning trap. The effective magnetic bottle produced from material of magnetization M placed around the trap center is given by the formula [11]

$$B_2 = 24\pi M \int \rho' d\rho' dz' r'^{-5} P_4(\cos\theta') \tag{2.30}$$

where $r^2 = \rho^2 + z^2$, and $P_4(cos\theta')$ is the fourth order Legendre polynomial.The insulator MACOR used in the trap has a paramagnetism of 0.78. By balancing the placement of material between the $P_4 < 0$ and $P_4 > 0$ regions (Fig. 2.4) B_2 can be minimized.

2.3 Quadrupole Potential

The trapping potential must remain harmonic over an extent away from the origin in order to have a well-defined axial frequency. The temporal variations of the spring constant must also be minimal for the same reason. Furthermore, any higher frequency noise (including thermal noise) will drive the particle and degrade the signal.

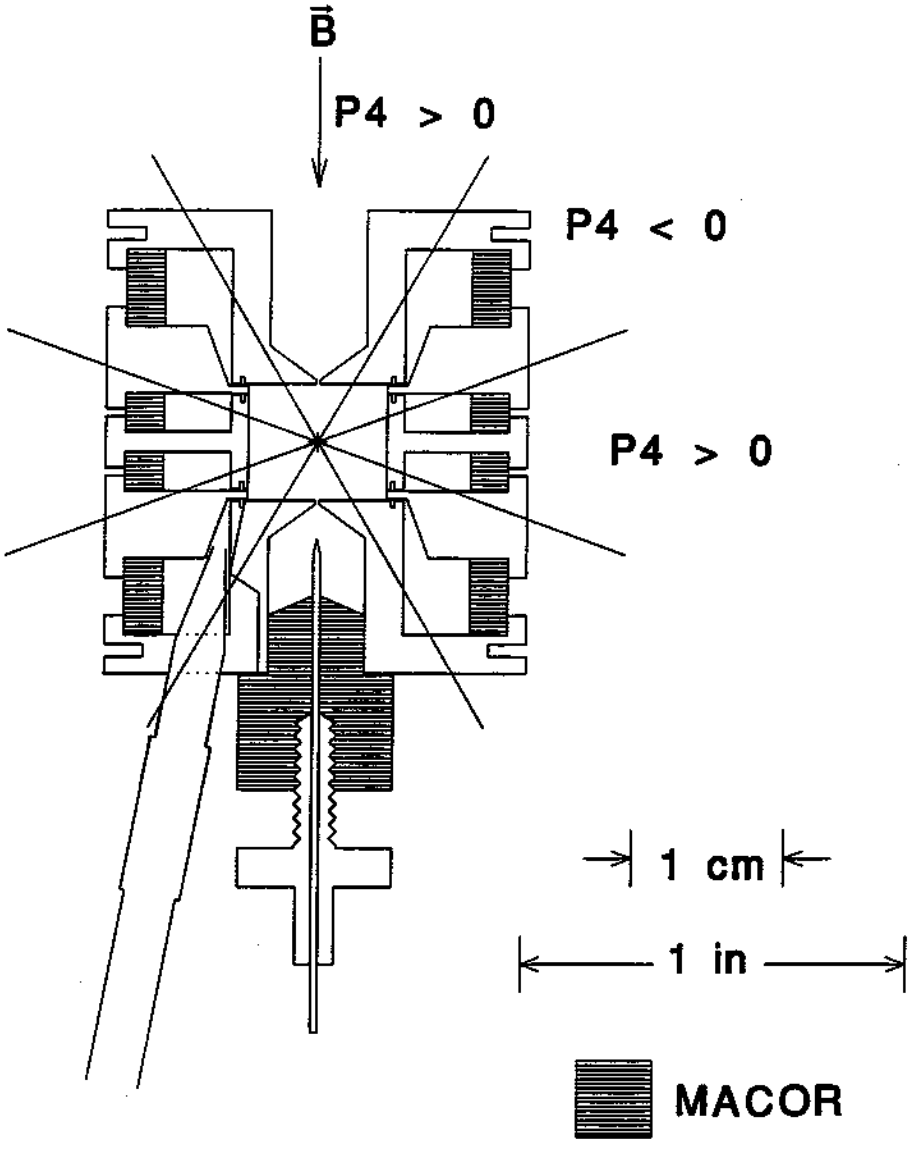

Figure 2.4: Lines separate regions of positive and negative paramagnetic contributions to the magnetic bottle in the cylindrical trap. Paramagnetic material such as MACOR is placed so as to minimize the overall quadratic gradient.

To obtain the most stable trapping potential, a set of ten cadmium-mercury amalgam unsaturated standard cells (Eppley 101) were connected in series inside a temperature regulated environment ($32.01°C \pm 0.01C°$, measured). The temperature coefficient is balanced between the positive mercurous sulfate limb and the negative cadmium limb, giving (from specifications) only $-18\mu V/°C$ at the set point temperature. This corresponds to a shift in the axial frequency of 1 Hz/C°. The time constant for a temperature change is typically much longer than a measurement of the axial frequency, the frequency may drift, but is not broadened. The batteries are attached to the trap via wires of a single material (Constantan) to avoid thermocouple effects. Since the electrodes are copper, there is a thermocouple junction where the Constantan wires are attached. However, the junction is maintained at 4.2 K, with a junction thermal gradient of less than $\pm 0.1K$, which corresponds to a negligible variation of $0.3\mu V$. Furthermore, the battery system and trap are enclosed in a faraday cage that shields both radiofrequency interference and thermal air currents. The voltage is finally filtered at liquid helium temperature by a large RC filter (10 second time constant) as well as by radiofrequency filters.

The trapping potential is electrically compensated [87, 35] to create as harmonic a potential as possible near the center of the trap. The particular geometry of the trap is chosen to orthogonalize [35, 42] the trap so that the axial frequency of the electrons is independent of the unavoidable adjustments in the compensation potential. There are two trap geometries discussed in this work: hyperbolic and cylindrical [77]. The hyperbolic geometry (Fig. 2.5)provides the larger volume of harmonic potential, and so may be best suited for large amplitude studies or for precision measurements. The cylindrical geometry (Fig. 2.6), on the other hand, permits an exact analytical solution of its cavity modes, (whereas, the hyperbolic geometry does not). Therefore, the interaction of the cyclotron oscillator with these modes can be studied in the cylindrical trap and compared directly with the calculations. Furthermore, the cylindrical geometry is easier to fabricate than the hyperbolic geometry. Indeed, the cylindrical trap has been shown to be suitable for precision measurements [77].

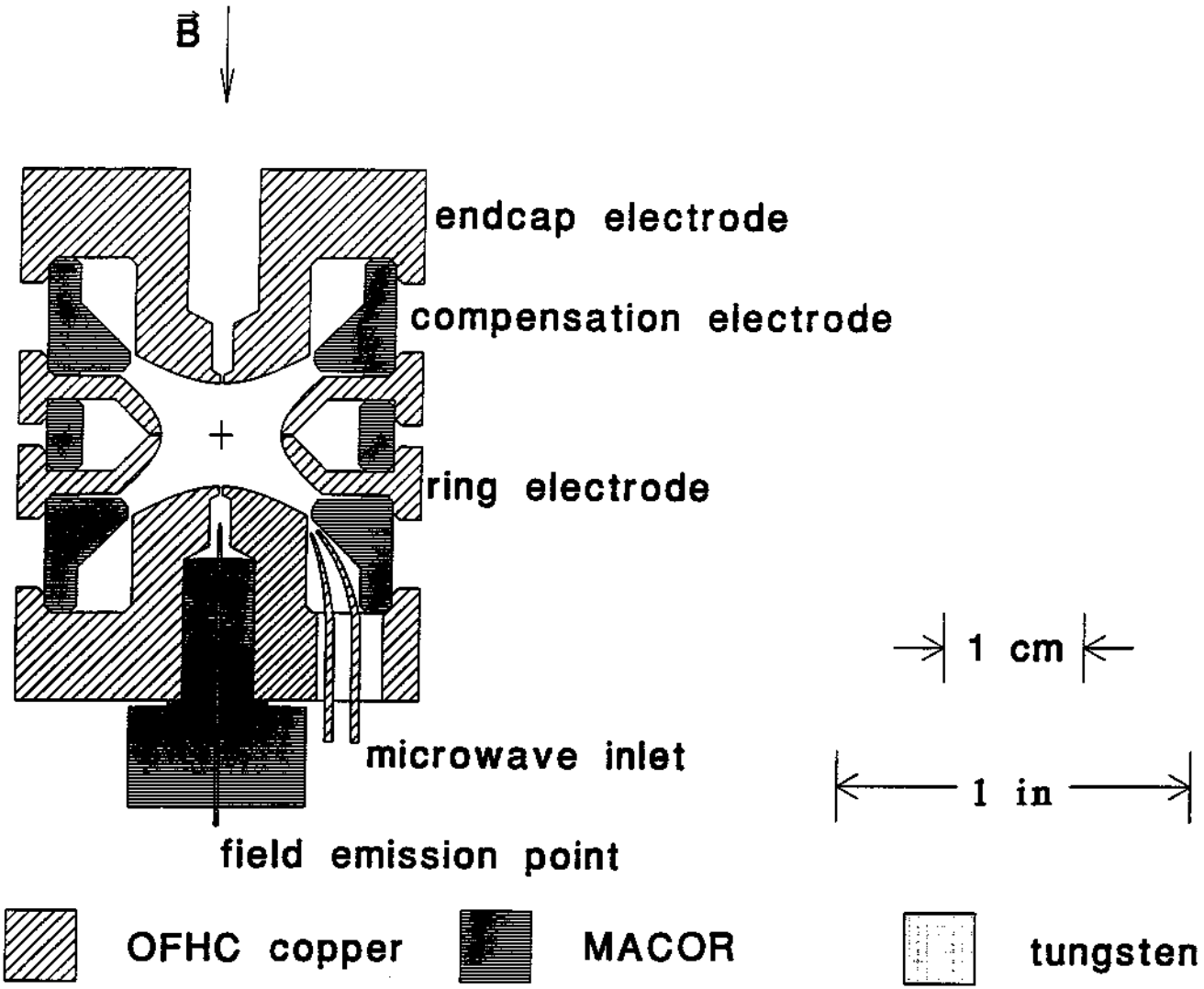

Figure 2.5: Orthogonalized hyperbolic Penning trap. The electrodes are formed along the hyperbolic equipotentials of a quadrupole potential.

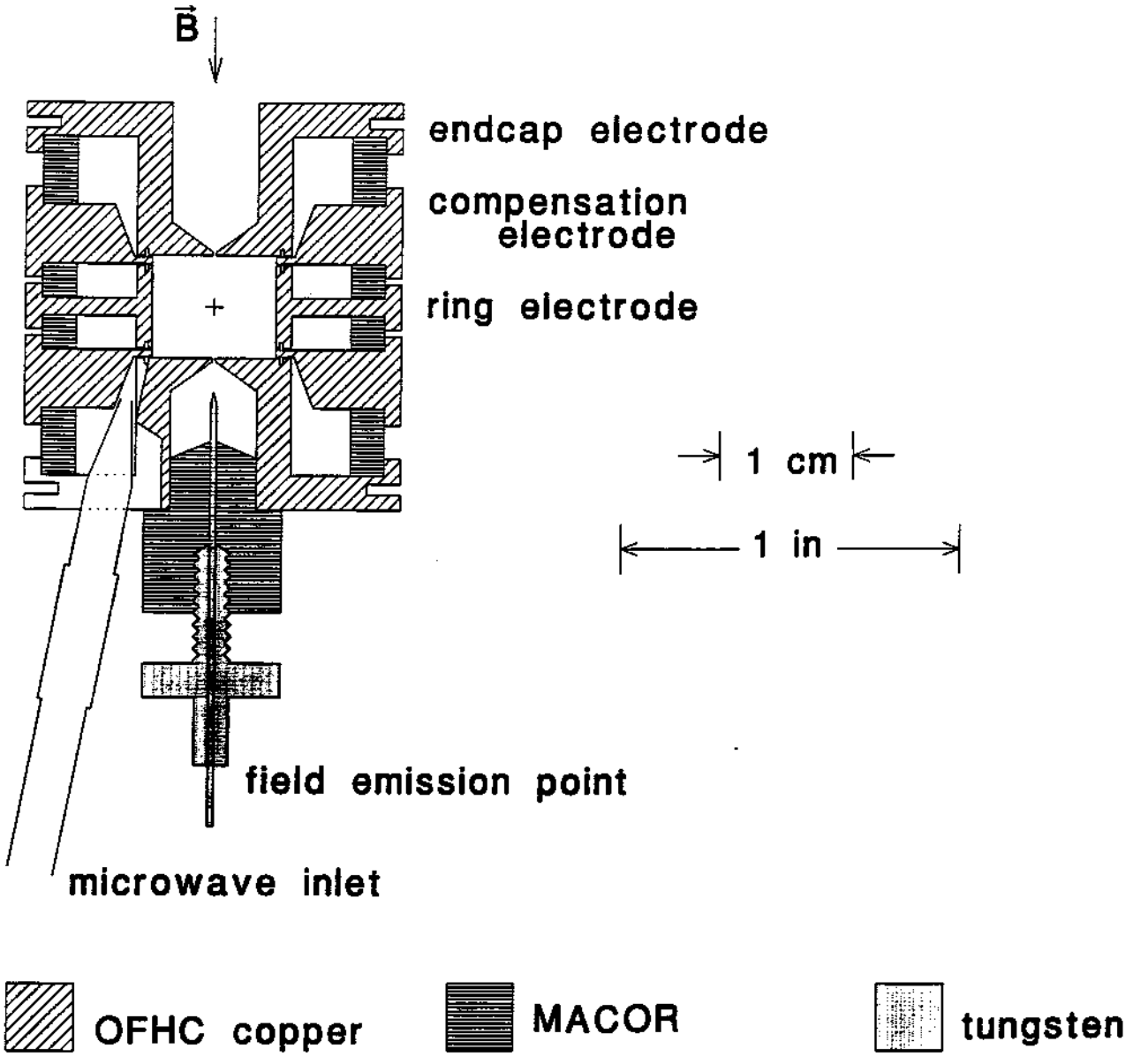

Figure 2.6: Orthogonalized cylindrical Penning trap. The electrodes form a high Q microwave cavity. Quarter-wave grooves act as choke flanges to minimize microwave radiation loss from the cavity.

2.3.1 Compensation and Orthogonalization

The Penning trap is electrically compensated to produce a harmonic trapping potential. With the appropriate choice of the relative electrode dimensions (orthogonalization), the axial frequency of the trapped particle becomes independent of adjustments in the compensation potential [35, 42]. These properties can be quantified as follows.

The potential within a Penning trap is

$$V = V_o\phi_o + V_c\phi_c, \tag{2.31}$$

where ϕ_0 is the dimensionless potential produced at the center of the trap with the compensation electrode boundary at value 0, the endcap boundary at 1/2, and the ring boundary at -1/2; and ϕ_c is the dimensionless potential produced at the center of the trap with the compensation electrode boundary at value 1, and the endcap and ring boundaries at 0. Near the center of the trap,

$$\phi_o = \frac{1}{2}\sum_{\substack{k=0 \\ even}}^{\infty}(\delta_{k2} + C_k^{(0)})\left(\frac{r}{d}\right)^k P_k(\cos\theta), \tag{2.32}$$

and,

$$\phi_c = \frac{1}{2}\sum_{\substack{k=0 \\ even}}^{\infty} D_k\left(\frac{r}{d}\right)^k P_k(\cos\theta), \tag{2.33}$$

where k must be an even integer because of the assumed invariance under rotations and under the reflection $z \rightarrow -z$. The characteristic trap dimension d is

$$d = \sqrt{(z_o^2 + \rho_o^2/2)/2}, \tag{2.34}$$

and δ_{k2} represents the harmonic part of the potential,

$$V_2 = V_o\frac{z^2 - \frac{1}{2}\rho^2}{2d^2}. \tag{2.35}$$

The coefficients of the expansion, that is, the potential, can be obtained using standard boundary-value techniques [35].

Writing the potential as

$$V = V_2 + \frac{1}{2}V_o \sum_{\substack{k=0 \\ even}}^{\infty} C_k \left(\frac{r}{d}\right)^k P_k(\cos\theta), \tag{2.36}$$

where k is an even integer. Thus,

$$C_4 = C_4^{(0)} + D_4 \frac{V_c}{V_o}. \tag{2.37}$$

For *anharmonicity compensation*, V_c should be chosen such that $C_4 = 0$.

The coefficients D_k measure the change in C_k for a change in V_c/V_o. Thus,

$$D_k = V_o \frac{\partial C_k}{\partial V_c}. \tag{2.38}$$

In particular,

$$D_2 = \frac{\partial \omega_z / \partial V_c}{\partial \omega_z / \partial V_o}, \tag{2.39}$$

since

$$\omega_z^2 = \frac{eV_o}{md^2}(1 + C_2). \tag{2.40}$$

Thus, D_2 is the relative sensitivity of ω_z to variations in V_c and V_o.

A D_2 of small magnitude is desirable. A large D_4 is also desirable to ensure that C_4 can be made to vanish for reasonable V_c insofar as

$$D_4 = V_o \frac{\partial C_4}{\partial V_c}. \tag{2.41}$$

This leads to the definition of a quality factor

$$\gamma \equiv \frac{D_2}{D_4}, \tag{2.42}$$

which goes to zero for an appropriate choice of ρ/z_o. Because the shape of the potential can be adjusted without changing the oscillation frequency for motion in this potential, traps with this property ($D_2 = 0$) have been called *orthogonalized*.

The orthogonalized cylindrical trap discussed here has the following parameters: $\Delta z_c/z_o = 0.2$, $\rho/z_o = 1.186$, $z_o = 0.3838$ cm. Furthermore, the coefficient D_2 has

coefficients	hyperbolic	cylindrical
z_0[cm]	0.3663	0.3838
ρ/z_0	1.160	1.186
D_2 measured	-0.000 3	0.000 02
D_4 calculated	-0.008 8	-0.07
$\gamma_4 = D_2/D_4$	0.03	-0.000 3

Table 2.1: Summary of dimensions and anharmonicity coefficients.

been measured to be 2×10^{-5}. Combining this with the calculated value for D_4, we have $\gamma = D_2/D_4 = -3 \times 10^{-4}$. This is to be compared with the values for previous hyperbolic traps: $\gamma_{hyp} = 0.56$, $\gamma/\gamma_{hyp} = -5.3 \times 10^{-4}$.

The values for the parameters in the orthogonalized hyperbolic trap are $\rho/z_o = 1.160$, $z_o = 0.3663$ cm, $D_2 = -3 \times 10^{-4}$, and $D_4 = -8.8 \times 10^{-3}$. This gives $\gamma = 3 \times 10^{-2}$. These and other coefficients can be measured in the hyperbolic trap using a new technique involving parametric oscillations. This will be discussed later in the chapter on the parametric oscillator. While the D_k parameters in the hyperbolic trap are only comparable to that of the cylindrical trap, the values for the C_k are much smaller, allowing the detailed study of the parametric oscillator. These are summarized in Table 2.1.

2.4 Cryostat

For a precision measurement of a single particle, it is essential that the ambient temperature be low for two reasons. First, the cryogenic temperature will provide an ultra-low vacuum, eliminating collisions with background gas atoms which would broaden resonance lines. Using the holdtime for antiprotons in a similar Penning trap, the background gas pressure was deduced to be better than 5×10^{-17} torr [40]. Second, thermal Johnson noise may overwhelm the motion of the particle and is directly detected. Even at an ambient temperature of 4.2 K, the typical amplitude of the directly driven axial excitation is only 10 times the thermally driven amplitude. Parametrically driven excitations are typically 33 times thermal. More importantly, the colder the black-body radiation background, the more the ground state of the cyclotron oscillator is occupied. At 4.2 K, the ground state is occupied 82 percent of the time. Work is underway in our laboratory to try to cool a Penning trap to millikelvin temperatures.

To minimize disturbances from refilling the cryostat with liquid helium the dewar was designed [79] to maximize the holdtime, which is how long the dewar can maintain the trap at 4 K. Furthermore, a low helium boiloff rate reduces thermal gradient disturbances due to gas flow out of the cryostat. To this end, great pains were taken to minimize any heat leak into the cryostat. Ultra-thin Constantan wires are used for electrical connections. The helium gas further cools the apparatus as it warms up to room temperature. This boiloff passes by a heat sink which is attached to a floating shield which equilibrates to a temperature between liquid helium and liquid nitrogen. A holdtime of six days was obtained without the FET heat load.

The cryostat used for the hyperbolic trap (Fig. 2.7) was made of solid copper. This has the advantage that the high thermal conductivity will keep the structure at a constant temperature profile, and thus constant length. The trap is thermally connected to the helium reservoir by copper rods.

The cryostat used for the cylindrical trap (Fig. 2.8) is an open-throated reservoir

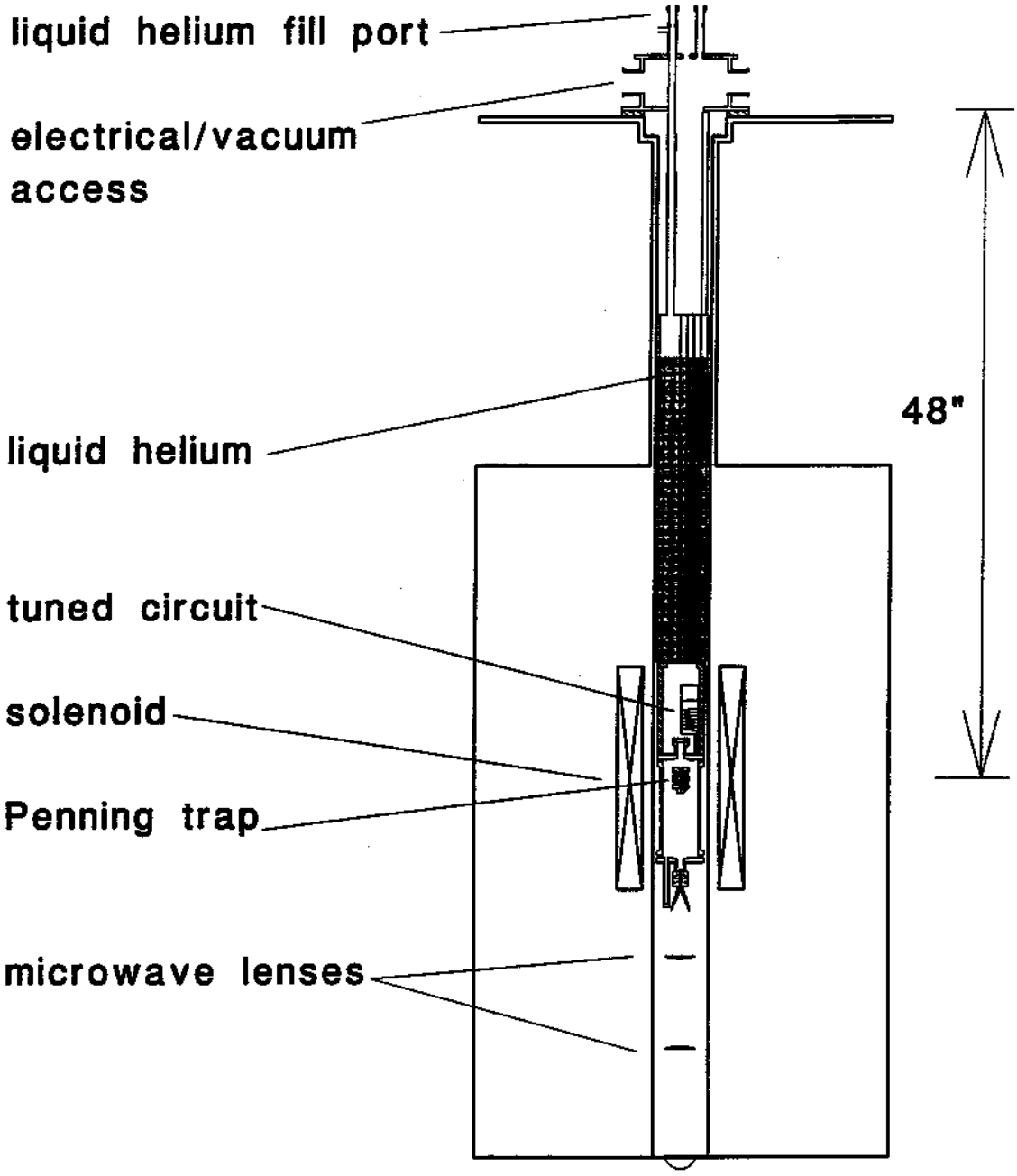

Figure 2.7: Liquid helium cryostat. The Penning trap is inserted into the bore of a superconducting magnet, and is cooled by thermal contact with the liquid helium dewar.

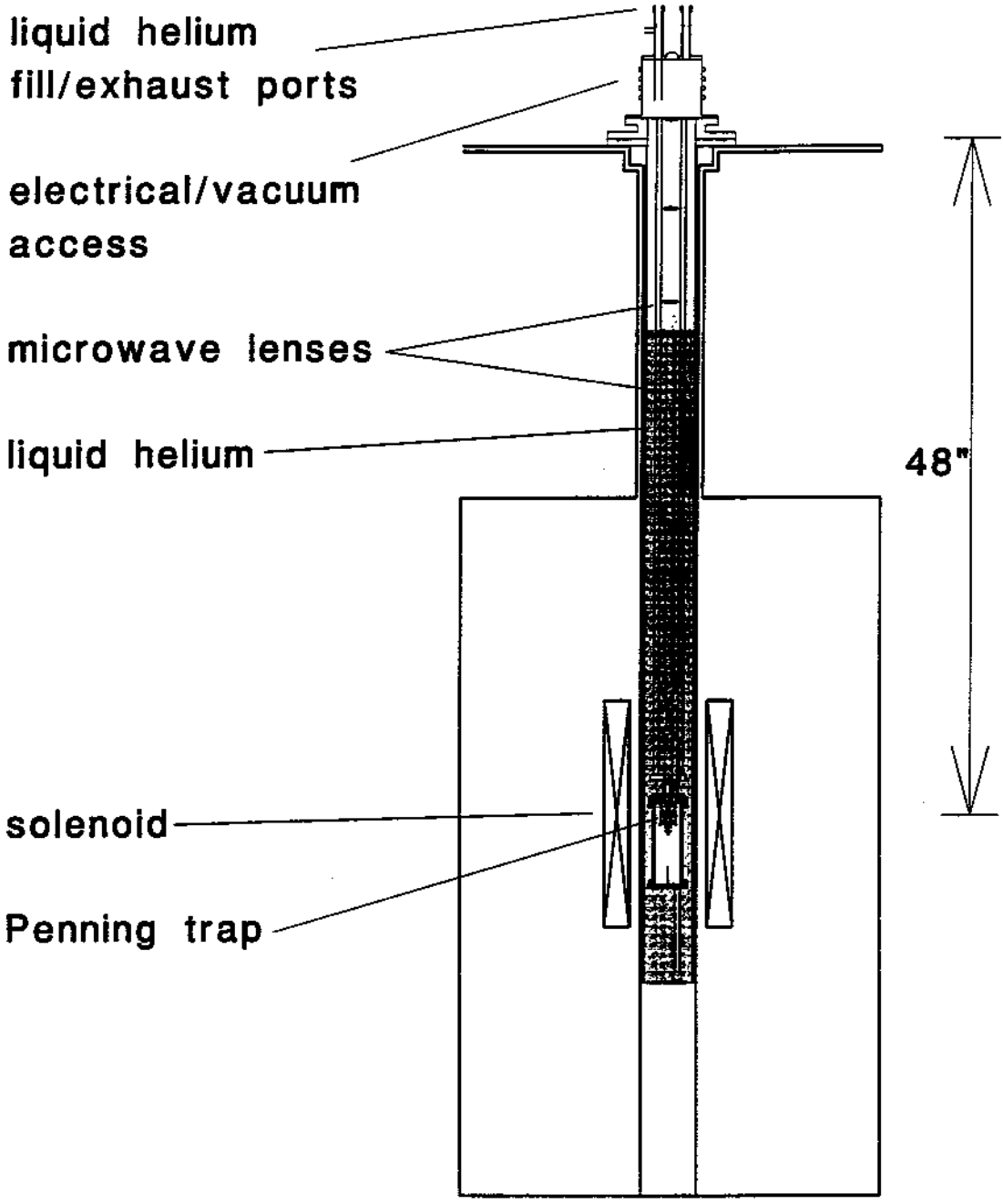

Figure 2.8: Liquid helium "bucket" cryostat. The cylindrical Penning trap is directly cooled by immersion in a liquid helium bath.

shaped like a bucket. The Penning trap, suspended on fiberglass rods is immersed directly into the liquid helium bath. This has the advantage of ensuring that all the components are at 4 K, or at least are very well cooled. Unfortunately, as the helium level changes over the course of the holdtime, the fiberglass supports thermally contract or expand, and shift the trap center in the field. As suggested in the section on the magnetic field, relative movement of the trap (with its paramagnetic contributions) and the solenoid may cause a change in the magnetic gradient environment.

2.5 Detection of A Single Electron

All information about the electron is gathered through the axial motion. By means of various couplings, information about the other degrees of motion can be written onto the axial motion. This is detected by means of sensitive radio-frequency electronics using a GaAs FET preamplifier which is cooled to 4.2 K. Different schemes are used to measure either the phase coherent signal or the power spectral density [29].

The detected signal is derived from the axial motion of the electron. The axial oscillations induce image currents in the electrodes, which currents flow through a resistor. This resistance is formed by adjusting an inductor so as to cancel the reactance of the trap capacitance, thereby leaving a purely resistive impedance. This resistance dissipates power, and acts to damp the motion of the electron. The voltage drop across the resistor is the detected signal which is fed to the input of the FET preamplifier, as shown in Fig. 2.9.

In order to obtain the best signal to noise ratio, the Q of the tuned circuit is made as large as possible. The Q of a circuit is defined as the ratio of the resonant frequency to the width of the response. The Q is proportional to the parallel resistance and thus inversely proportional to the damping constant. The coupling of the particle to the detection circuit can be adjusted by detuning the resonant frequency of the axial oscillations from the resonant frequency of the tuned

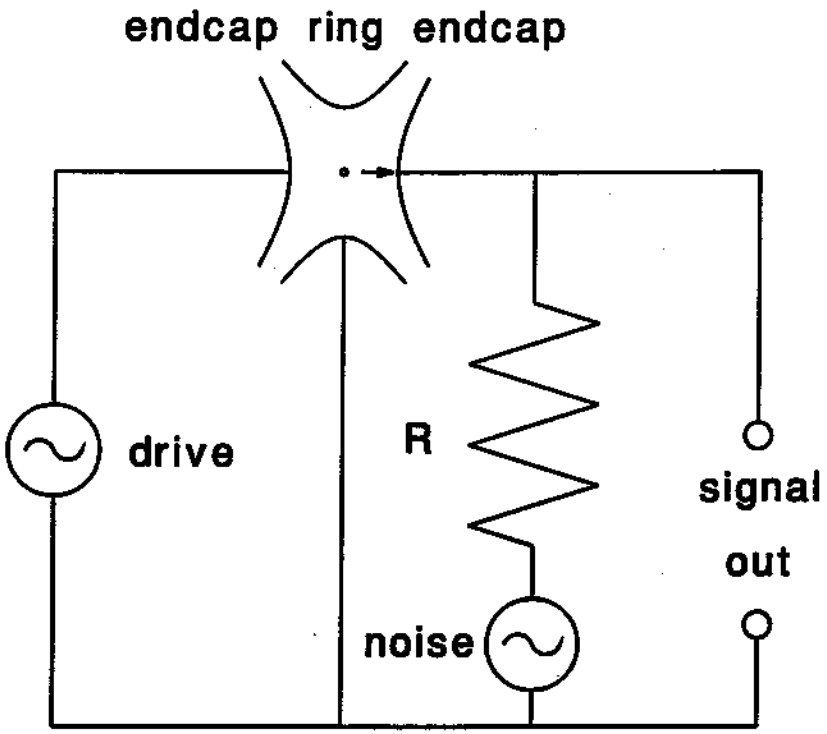

Figure 2.9: Drive and detection schematic. The effective resistor, R, is formed by an inductor and interelectrode capacitances.

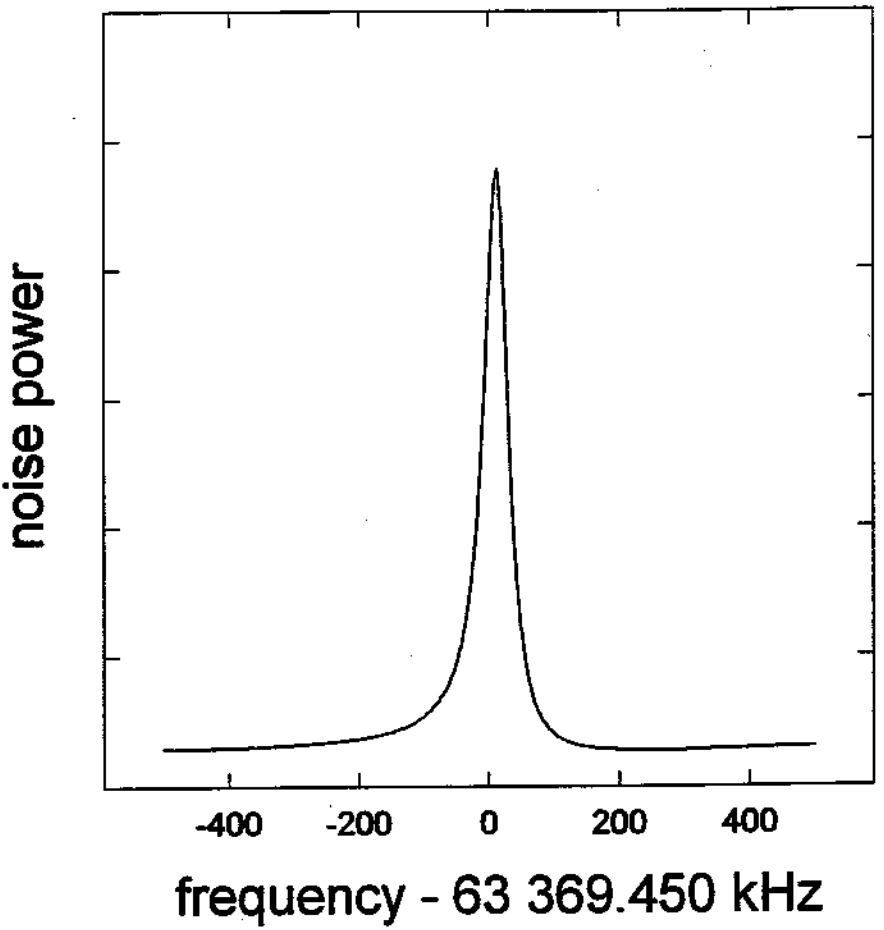

Figure 2.10: The liquid helium Johnson noise response of the tank circuit. The Q is about 1600.

circuit (Fig. 2.10).

The electron is driven by the thermal noise from the detection circuit and by an externally applied drive voltage. The electron axial oscillator itself can be modelled by an inductor and capacitor [92, 89]. On resonance, the effective impedance is zero and will short the noise voltage from the detection circuit. This gives rise to a 'dip' feature on the tuned circuit noise response (Fig. 2.11). The width is given by the axial damping constant. When the electron axial oscillator is driven by an external voltage, the response is a Lorentzian. Since the signal is the sum of the noise response and the driven response, noise shorting can be observed on resonance here as well. That noise shorting can be seen at all indicates that the axial frequency is defined well enough by a stable and harmonic axial trapping potential. The previous observation of noise shorting indicated a factor of two reduction; here almost a factor of six is observed. To help insure that the electron is actually at 4 K, the electrical leads to the trap are passed through cold (liquid helium temperature) attenuators, thereby reducing the thermal Johnson noise from the equipment at room temperature.

The 63 MHz signal from the tuned circuit is tapped off of the inductor coil (step-down ratio 6:1) and ac coupled to gate 1 of a dual gate GaAs MOSFET (Mitsubishi MGF-1100) which is cooled by thermal contact to the liquid helium reservoir at 4.2 K. This preamplifier is intended to isolate the electron from the following stages of amplification. The signal is then amplified and mixed to a convenient IF (5 MHz). This signal is then processed either by phase sensitive detection using a lockin amplifier (EG&G PAR 5202) or by power spectral density detection (power per unit bandwidth) using an audio spectrum analyzer (SRS 760 or HP 3561A). The lockin amplifier gives the familiar in phase and quadrature responses to an external drive. It also can give the equivalent magnitude and phase responses. The external drive on the endcap electrode is actually offset by 5 MHz, with 5 MHz being applied on the ring electrode in order to frequency modulate the trapping potential. This heterodyne technique is used to avoid direct feedthrough of the drive to the detection

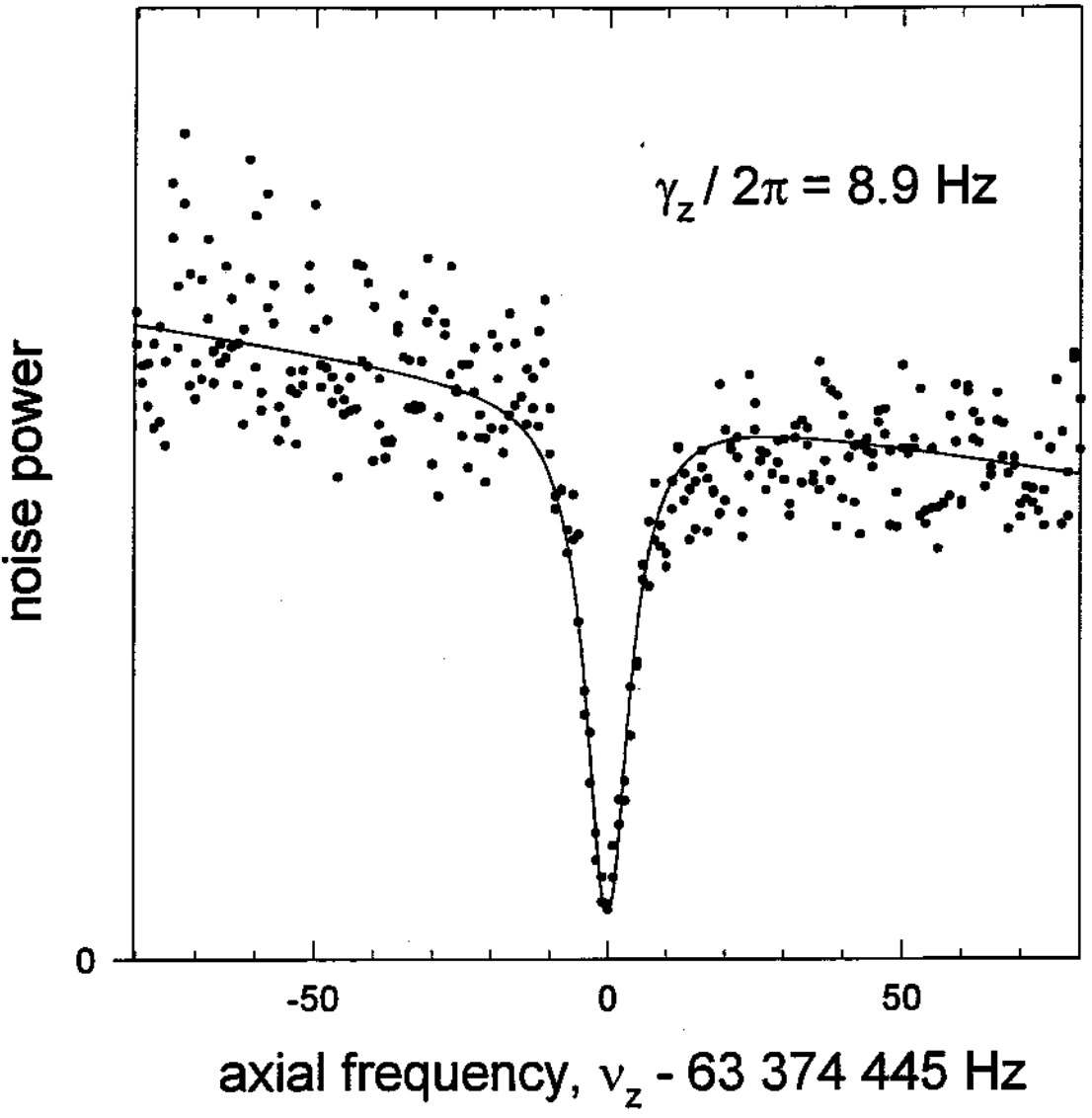

Figure 2.11: 4.2K Johnson noise shorting due to a single electron.

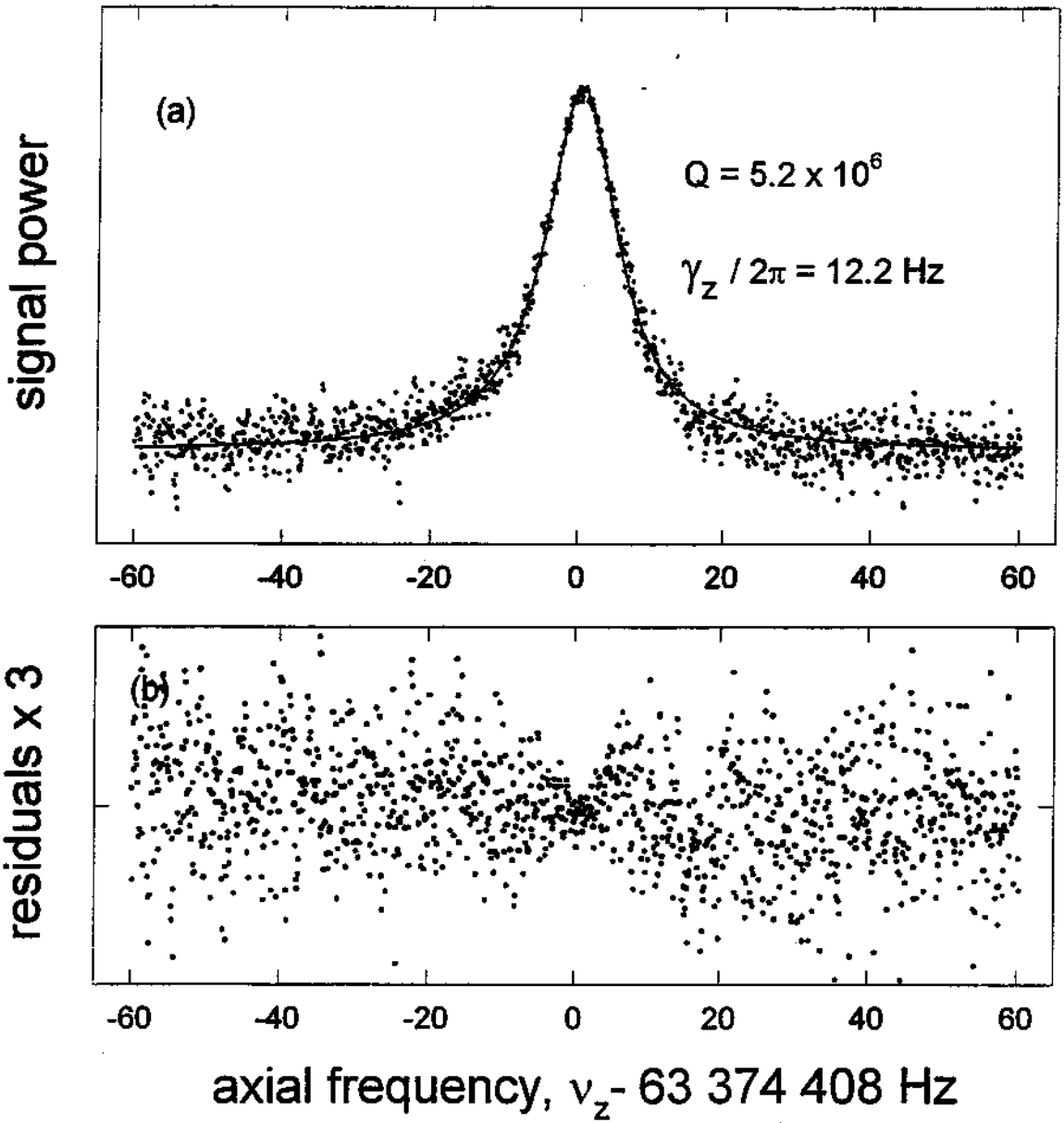

Figure 2.12: Driven axial response of a single electron. The residuals show that the Johnson noise is shorted on resonance. Typically, the driven axial amplitude ($z = 0.29$ mm) is 10 times the thermal amplitude ($z = 0.03$ mm). The parametric amplitude is about $z = 1.0$ mm.

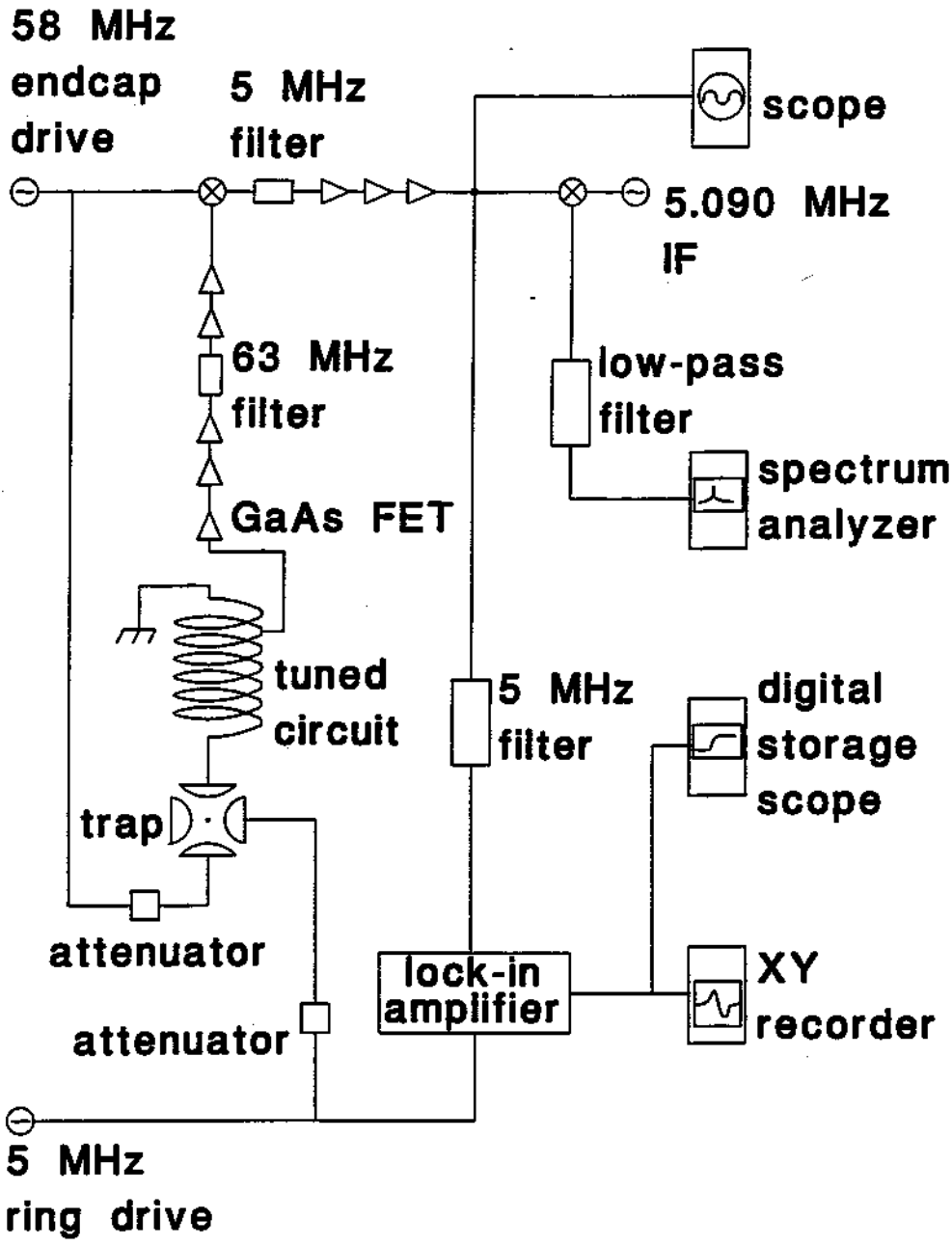

Figure 2.13: Drive and detection circuits. The phase coherent response of the axial motion to a drive is detected by a lockin amplifier. The power spectral density of the driven or undriven motion can be detected using an audio spectrum analyzer.

circuitry. The set up is summarized in Fig. 2.13.

The detected axial signal is used to determine the exact number of electrons loaded into the trap. One electron may be loaded using the following procedure. An electron beam from a field emission point (a sharpened tungsten wire) follows a field line into the trap, and dislodges some atoms from a surface at the back of the trap. Another electron then scatters off an atom or is stripped from the atom. A low energy electron that is generated may then be trapped. As electrons are confined within the trap, the number may be inferred from the number of discrete steps in the detected axial signal during the loading process. The signal is detected far off resonance where it is insensitive to the detail of the anharmonicity in the trap and where, for an appropriate phase in the detection circuit, the signal is directly proportional to the number of particles. Once the step size for an electron has been determined, the trap is then purged, and one electron loaded.

2.6 Microwave Source

In order to measure the cyclotron frequency to a high precision, the microwave drive must be sharp in frequency space, or at least have a sharp feature. Since the cyclotron frequency is determined by the magnetic field, stability in the magnetic field seen by the electron will determine the stability of the cyclotron frequency. Thus, motion through a magnetic field gradient will be equivalent to a varying cyclotron frequency. Conversely, noise on the cyclotron drive can be treated as motion through a magnetic field gradient.

The relativistic cyclotron excitation (discussed in the next chapter), requires a microwave source with an extremely low phase noise spectrum. This relativistic motion is particularly sensitive to phase noise near 1 kHz. This corresponds to the "bucket frequency" for small oscillations in phase space about the stable attractor, which will be discussed in Chapter 4.

The cycloton motion of an electron in a 6 Tesla field is at 164 GHz. This is in

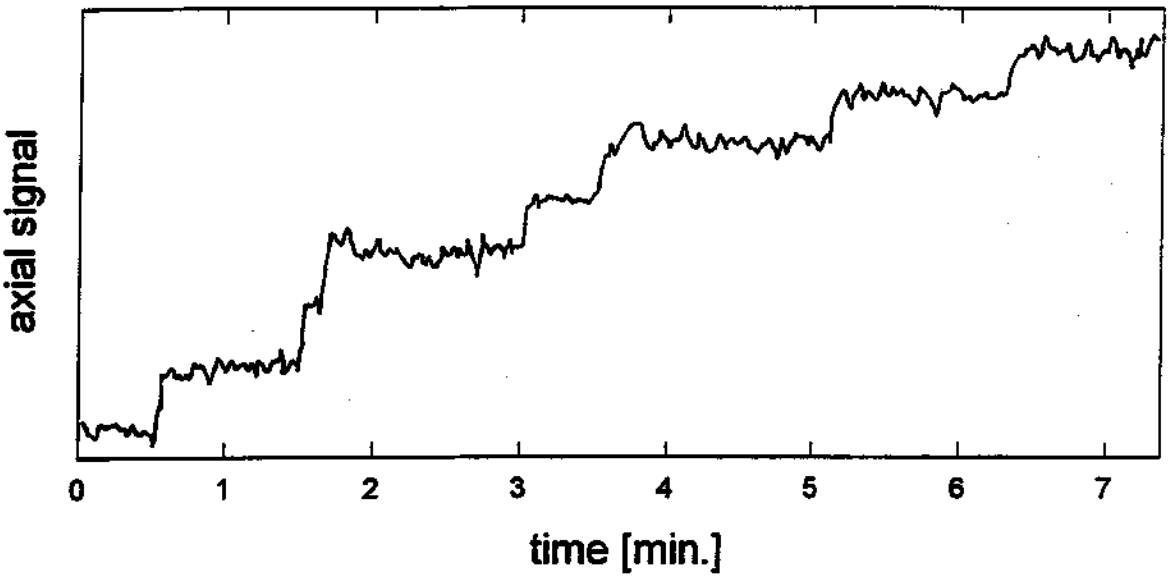

Figure 2.14: Discrete loading of electrons. It is evident that there were 7 electrons trapped.

the D band of the microwave spectrum (110-170 GHz). The microwave source is synthesized beginning with a stable 10 MHz crystal, which is then multiplied up to the X band (10.24 GHz). This is the long-time stable reference source that is mixed with 360 MHz (frequency locked to the 10 MHz crystal) to phase lock, with a long time constant, a 10.6 GHz cavity oscillator which is stable over short time scales because of a fast phase lock loop. This is then mixed with a tunable 750 MHz oscillator to produce a frequency near 11 GHz, which is then multiplied by a factor of 13 in a harmonic mixer up to the D band.

2.6.1 10.24 GHz Reference

The microwave source is referenced for long term stability to a hand-picked, 10 MHz "BVA" crystal from France. This crystal is located inside a Hewlett-Packard Model 8663A Synthesized Signal Generator (option H40). From this 10 MHz crystal, 640 MHz is internally synthesized within the HP 8663A and output to a rear sma type connector at a level of 0 dBm. This 640 MHz signal is sent to a steel box containing the X band stages. The steel box provides some magnetic as well as vibrational and acoustical shielding. Isolation transformers (1:1) are used in passing signals through the steel enclosure in order to suppress 60 Hz noise. Within the steel box, the signal is amplified by 12.5 dB before passing through a bandpass filter centered around 640 MHz. The signal then is amplified by 27 dB. The power amplifier is again filtered at 640 MHz before being matched through a -3 dB pad into a step recovery diode. This diode is a custom built impulse train generator (Hewlett-Packard model 33004A, option H26) matched for 50 Ω at 640 MHz. This produces a comb of frequencies at harmonics of 640 MHz. The input to the diode is about +21 dBm, which produces an output at 10.24 GHz of -20 dBm. The 16th harmonic at 10.24 GHz is passed through a section of X band waveguide (which serves as a high pass filter), and then through a pair of filters of width 250 MHz. These are isolated with circulators (ferrite devices) to prevent reflections from the filters. Finally, this is

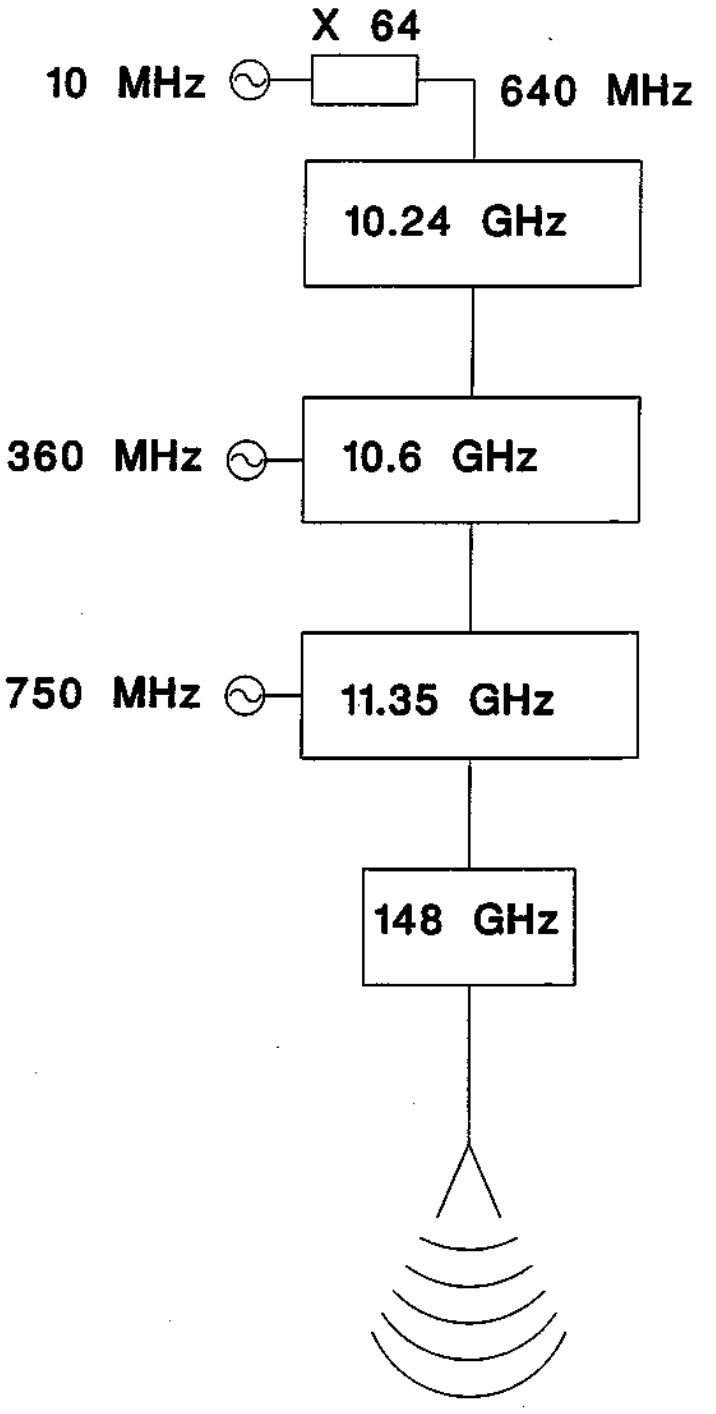

Figure 2.15: Overview of microwave system.

passed through a dc block into the 10.6 GHz section.

2.6.2 10.6 GHz cavity

The 10.6 GHz source was constructed by F.L. Walls of the National Institute for Standards and Technology in Boulder, Colorado. It utilizes a lead-coated iridium cavity with a loaded Q-factor of about 20,000. The cavity is stabilized with two phase locked loops. There is a fast loop which mixes the output of the cavity with the input and sends the resulting error voltage to a varactor controlling the 10.6 GHz source. The slow loop mixes the output of the cavity with the multiplied reference which is synthesized from the 10.24 GHz and a 360 MHz LO. This passes through an integrator and a variable gain op amp circuit, and then to the 10.6 GHz varactor. The loop saturates at ±5 Volts with a slope of 5 kHz/Volt with respect to the 10.6 GHz output. The whole assembly is maintained at a temperature of 55°C. The temperature coefficient is about -10 kHz/C°.

Three tests of the noise of the source were performed by our collaborator, Fred L. Walls. There were two different tests of phase noise, and one of amplitude noise. The first phase noise test used a high-Q cavity (loaded Q = 25,000) in a frequency discriminator circuit. The 10.6 GHz source was injected into the cavity and the output was compared to the input (phase shifted) with a double balanced mixer. The resulting DBM output was recorded versus the frequency of the phase noise. The overall sensitivity k was 4.97×10^{-5} Volt/Hz. The measurements were taken well within the half width of the resonator. The phase noise power is given by the modulation index squared divided by the bandwidth. The modulation index is defined as the maximum deviation over the modulation frequency, f. For small deviations, then, the phase noise power is

$$S_\phi = \frac{V^2/k^2 f^2}{BW}. \tag{2.43}$$

The second test compared a pair of 10.6 GHz oscillators. Again, the slope of the zero-crossing gives a measure of the phase noise sensitivity. The measurements were

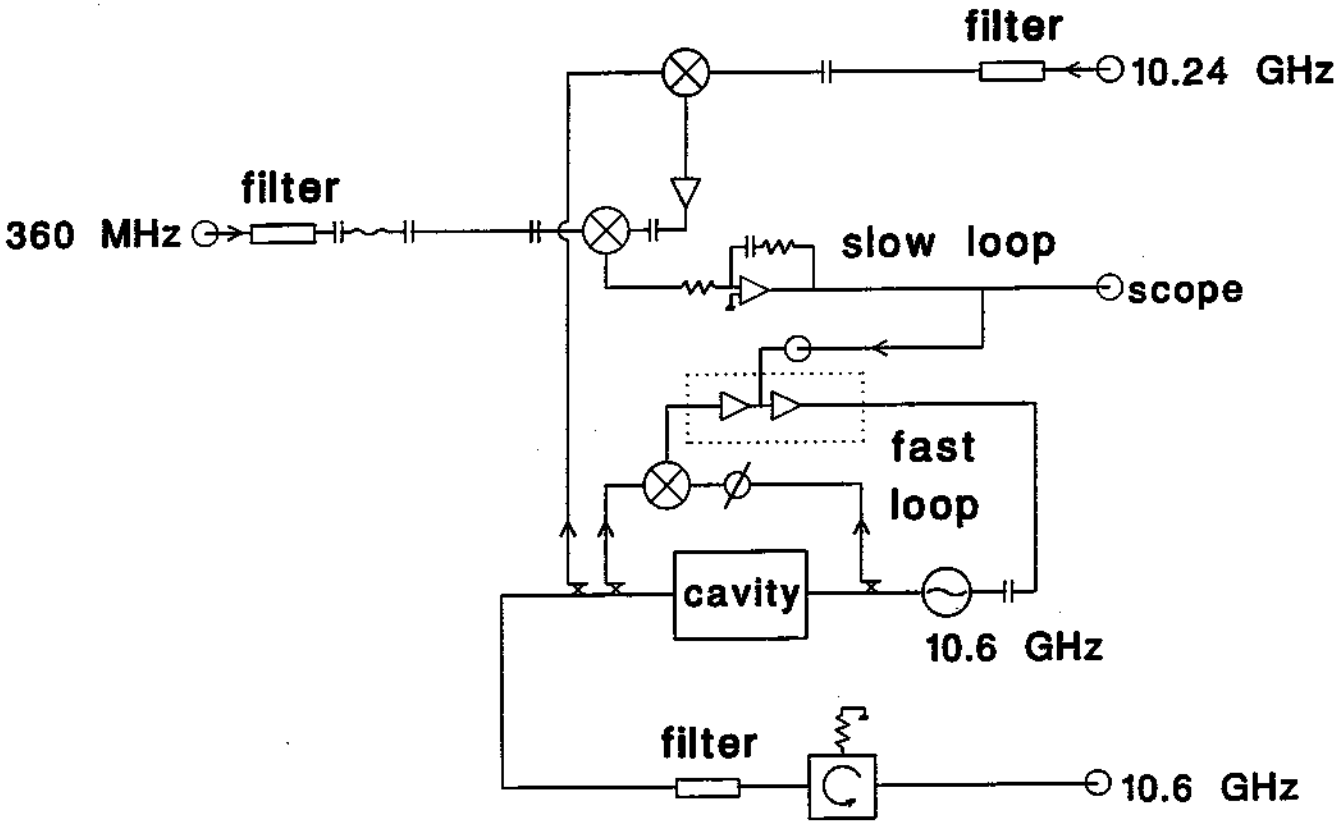

Figure 2.16: Schematic of 10.6 GHz system.

checked by measuring the amplitude noise as well, which is expected to be roughly the same as the phase noise far off from the carrier. The measured phase noise of the 10.6 GHz system and of the 10.24 GHz system are shown in Fig. 2.17.

2.6.3 Slow Phase Lock Loop

Long term stability is provided by the crystal based 10.24 GHz system, whereas short term stability is provided by a 10.6 GHz phase locked cavity. These two are interfaced through a lock loop with time constants chosen so as to reflect the 10.24 GHz stability close in to the carrier, and the 10.6 GHz spectral purity far off the carrier, as shown in Fig. 2.17.

The transfer function of the circuit shown in Fig. 2.18 is given by

$$G(\omega) = \frac{-K(i\omega + \omega_1)}{(i\omega)^2(i\omega + \omega_2)(i\omega + \omega_3)} \tag{2.44}$$

where $\omega_1 = 1/R_2C_1$,$\omega_2 = 1/R_2C_2$, $\omega_3 = 1/R_4C_3$ and $K = ig\alpha/R_1C_2R_3C_3$. The unity gain frequency,

$$\omega_u = \frac{K}{\omega_2\omega_3}. \tag{2.45}$$

is roughly the inverse of the response time of the loop. For stability, the phase shift at the unity gain frequency must be much smaller than 180°. The poles and zeros shown in Fig. 2.19 are chosen such that the unity gain point has a slope of 6 dB/octave (90° phase shift), and that the other poles are spaced apart by roughly a factor of four (critical damping at $\omega_1 = \omega_u/4$).

2.6.4 IF Section

The 10.6 GHz output is mixed with a small IF of about 750 MHz from the front panel of the HP8663A synthesizer to obtain 11.35 GHz. Thus, the frequency of the output can be easily controlled by changing the frequency of the IF input. The mixer is driven in saturation (which occurs around 0 dBm). The signal then passes

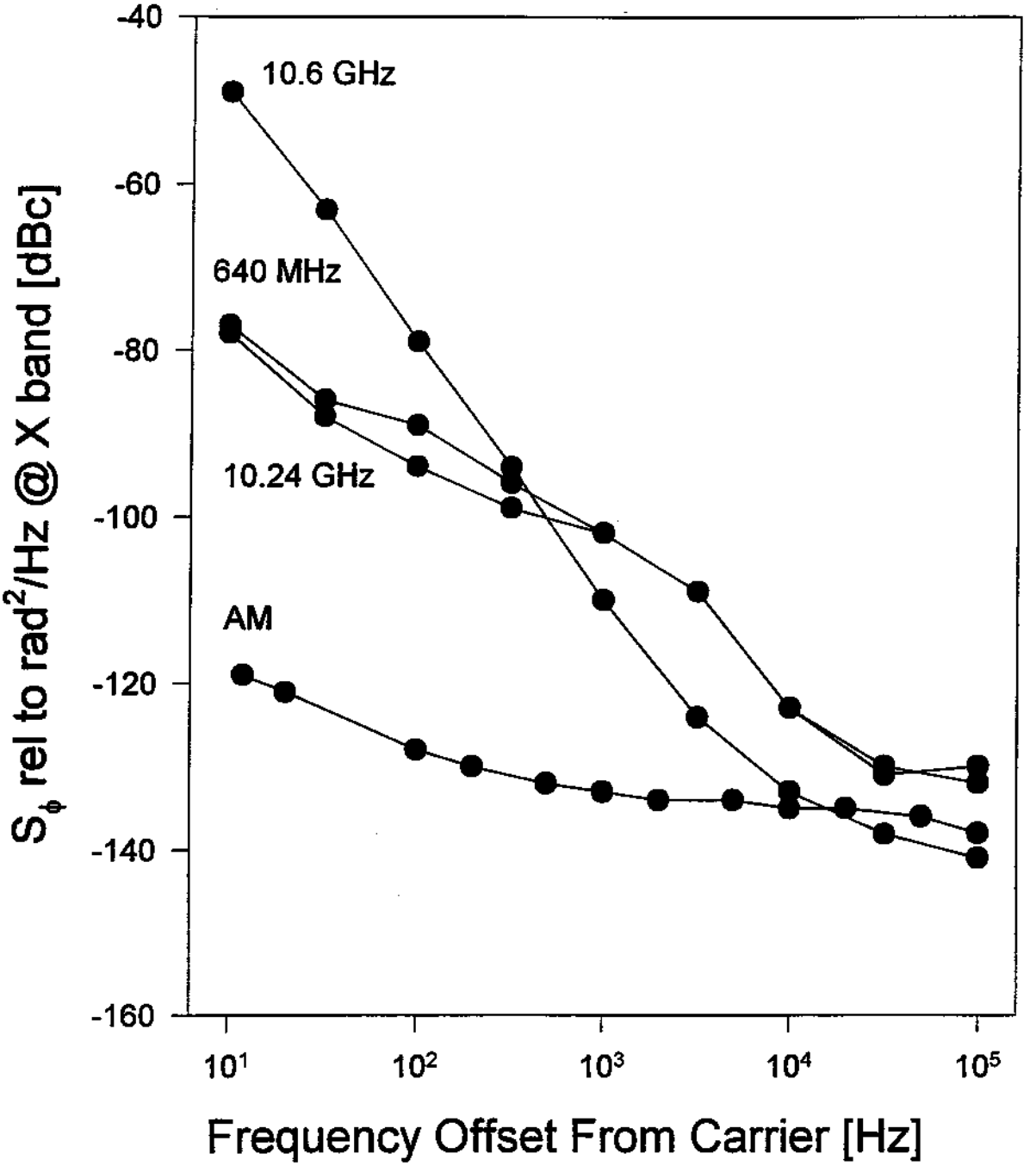

Figure 2.17: Phase noise measurements on the 10.6 GHz and 10.24 GHz systems. The two systems are interfaced with a phase lock loop such that the final phase noise is that of the 10.24 GHz system close in to the carrier, and that of the 10.6 GHz system far from the carrier.

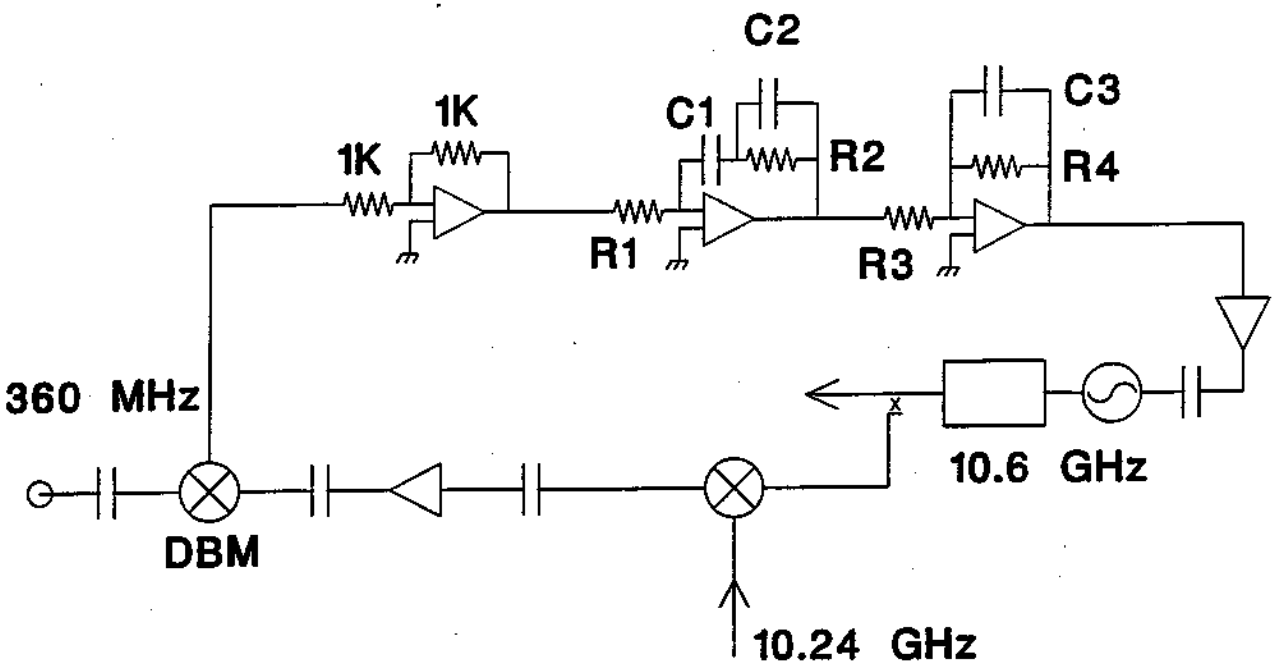

Figure 2.18: The slow phase lock loop. The time constants are set by the RC values. R1=10K, R2=10K, R3=10K, R4=4.7K; C1=0.3μF, C2=0.01μF, C3=5600pF.

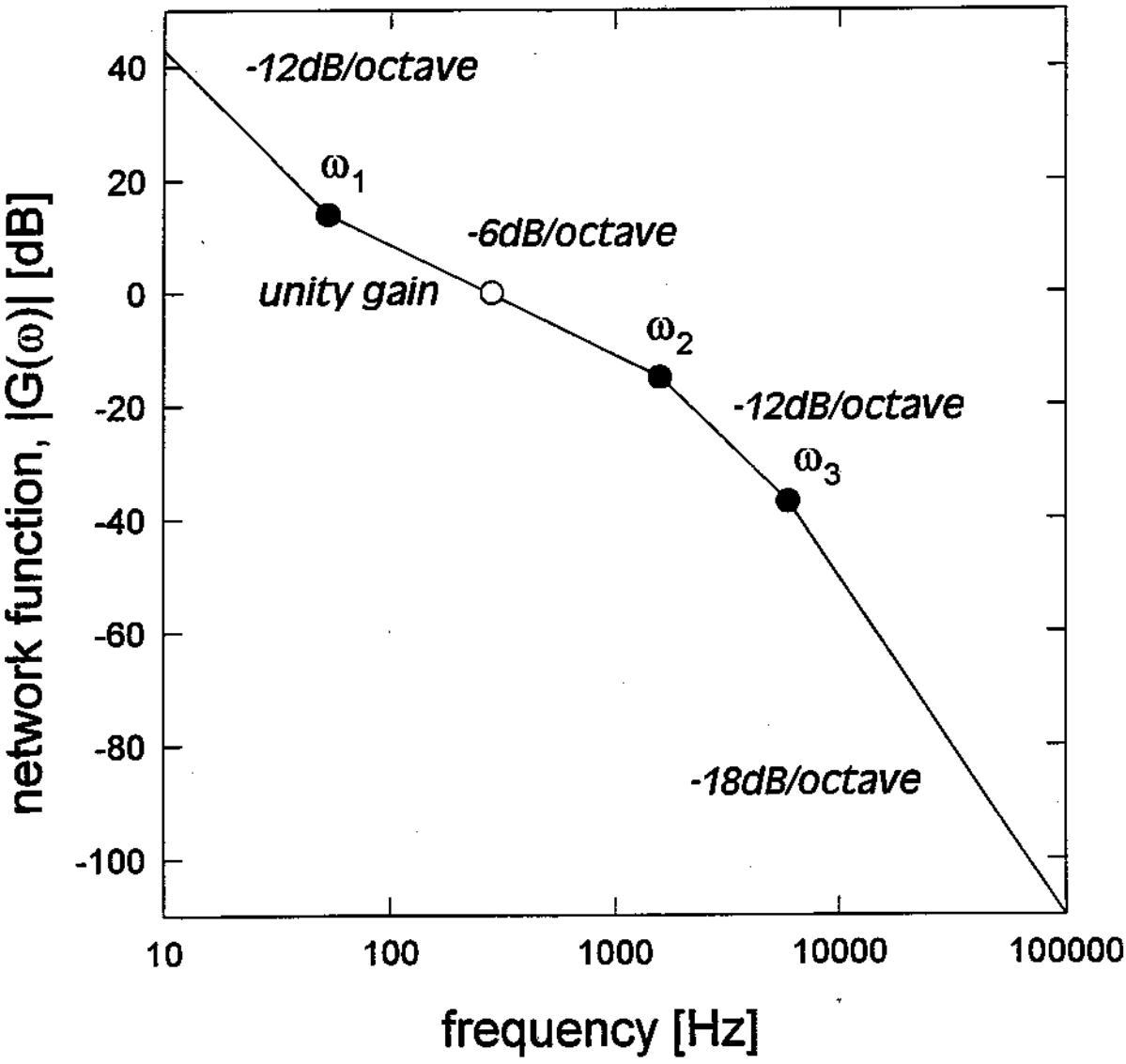

Figure 2.19: The measured bode plot for the slow phase lock loop. The unity gain frequency is at 282 Hz, at a slope of -6 dB/octave.

through a circulator before being filtered by a seven pole filter with a passband of 340 MHz between 3 dB points. This suppresses the 10.6 GHz carrier, as well as the lower mixed sideband. The signal is then amplified and filtered again before being boosted by a power amplifer to a level of +18 dBm.

2.6.5 D band Section

The X band output of the last section is used to generate D band radiation through a harmonic mixer (Alpha 922FX0HN). This contains a GaAs Schottky barrier diode as a non-linear element. The diode produces a comb of frequencies (typically, the 13th, 14th, or 15th harmonic is used). The IF port of the mixer is terminated with 50 Ω. The power was optimized by adjusting the impedance seen by the bias port. The maximum seemed to occur at 180 Ω. The mixer also has a tuning stub which maximized the power at about a half an inch out. The optimization is shown in Fig. 2.22. An inductor within the case of the mixer was tuned by the manufacturer to adjust the LC matching, and we found that different batches of diodes gave different maximum output powers. The conversion loss to the D band is given by the curve shown also in Fig. 2.22. This was measured with an external mixer interface (HP 11970 harmonic mixer, HP W365A isolator, and HP 70907A interface). This has a conversion loss of -70 dB at 164 GHz. Various isolators and straight sections of waveguide were inserted to check for reflection resonances. None were found. The maximum power obtained was -92 dBm detected power, or -22 dBm at the mixer output.

The D band power can be reduced in a precise way using a calibrated attenuator (TRG 523/716). This device is a micrometer driven mica vane with a resistive coating that is inserted into the waveguide interior. The power absorbed is related to the insertion depth. This allows attenuation values from 0 to 25 dB. The D band radiation then passes through a gain standard horn (TRG D861, 25 dB) into a series of teflon lenses which guide the radiation from the room temperature setup

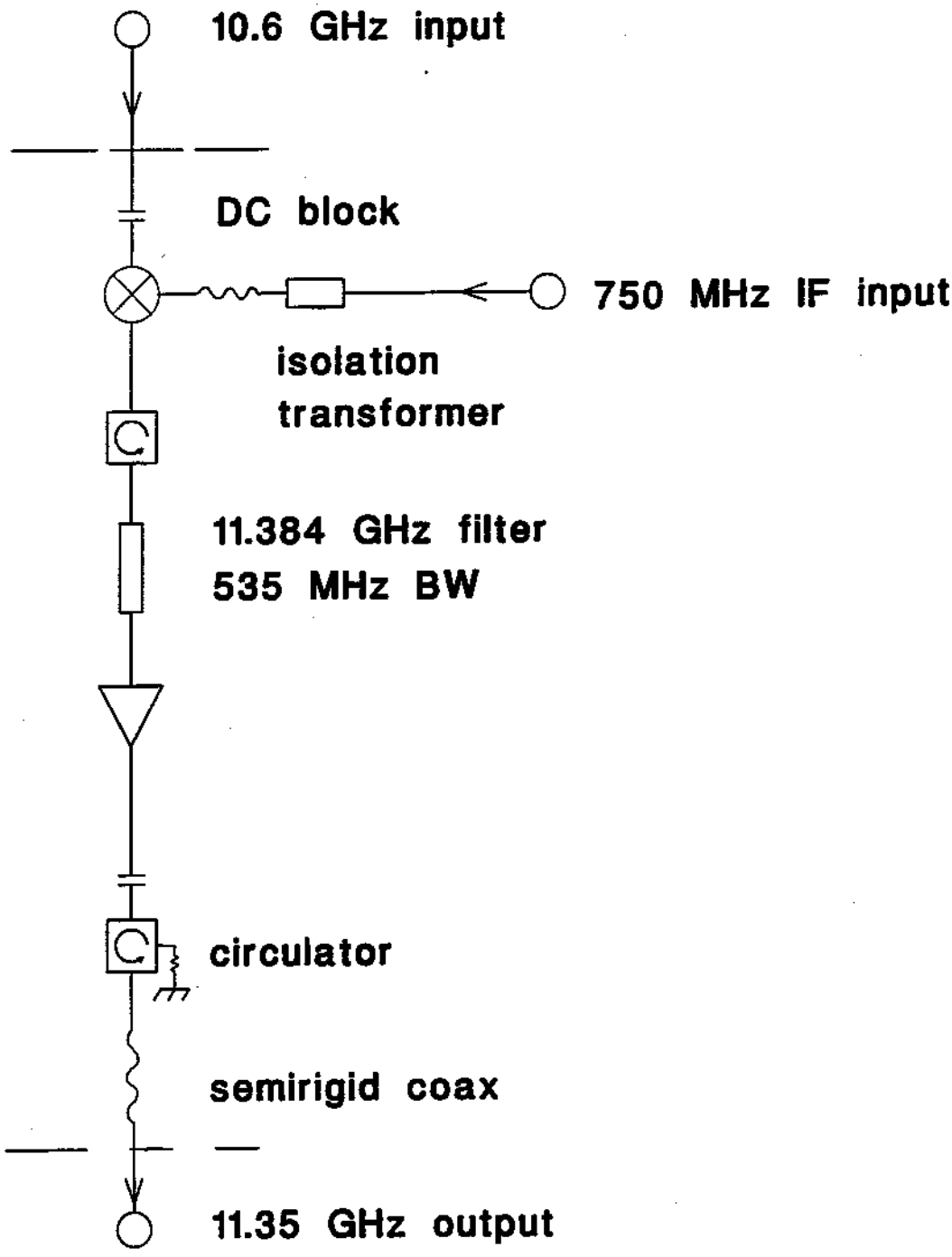

Figure 2.20: A 750 MHz input allows variation of the final microwave output frequency.

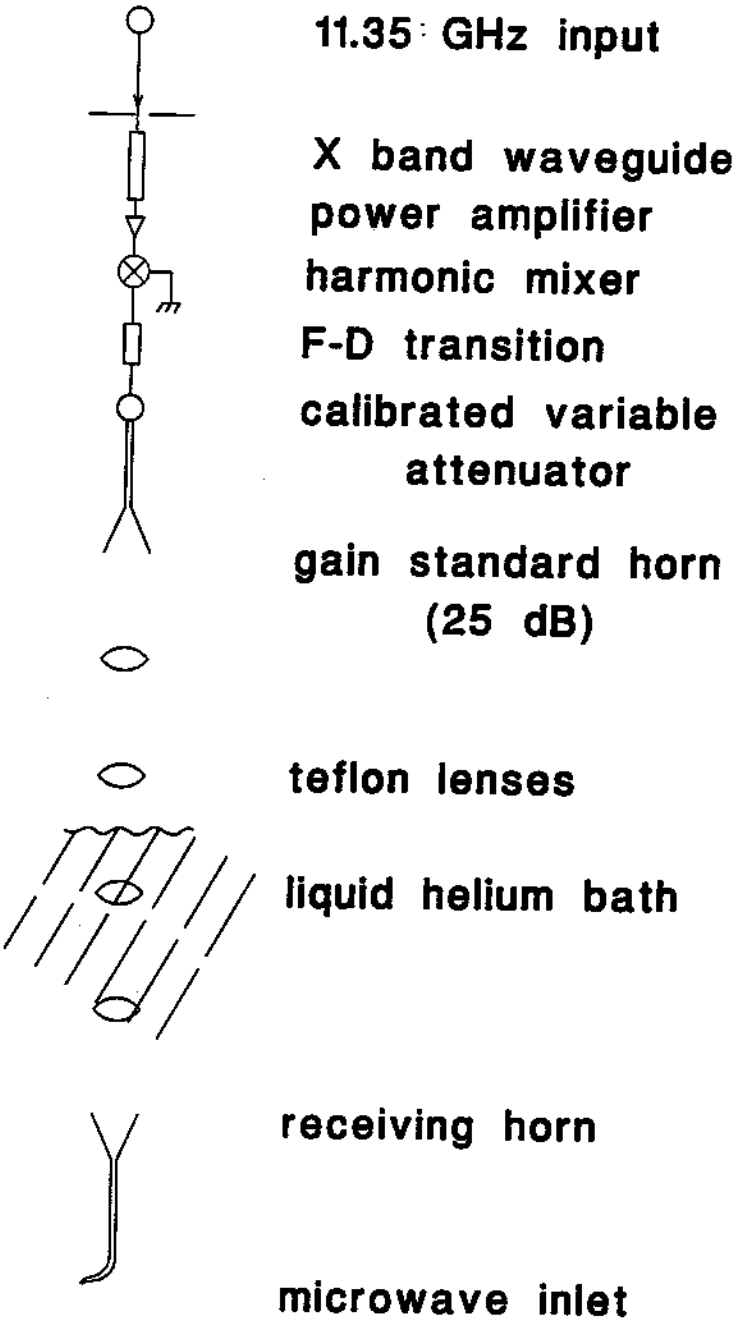

Figure 2.21: Schematic of D band section.

to the liquid helium environment of the Penning trap. The last lens matches into an oversized circular waveguide and into the trap interior.

We measure that modulation of the X band input produces a modulated D band output that follows the expected Bessel function dependence of the sidebands. That is, for a given modulation index, x, the n^{th} sideband will have an amplitude equal to $J_n(x)$. The modulation index is defined to be the ratio of the peak deviation from the carrier (ML) to the modulation frequency. We take the deviation at D band to be the X band deviation multiplied by the upconversion factor. The modulation behavior is not immediately obvious due to the non-linear power dependence of the harmonic mixer diode. A modulated microwave source is a useful tool in examining the relativistic anharmonic oscillator, as will be discussed later.

2.7 Portable Penning Trap

Not only is the hyperbolic Penning trap sensitive enough to detect a single electron, but it is also robust enough to transport particles over long distances [80]. (Charged particles are routinely stored in a Penning trap for long times. For example, a single electron was stored continuously for over ten months [39].) This robustness is of more general interest for moving antimatter. For example, greater precision measurements could then be done on antiprotons that were moved away from the magnetic disturbances of the accelerator (LEAR) from which they were produced [40]. They could also be used in experiments involving large immovable detectors (e.g. hadron spectroscopy experiments) with greater resolution than possible with the detectors located at LEAR. Furthermore, the antiprotons could be reaccelerated in another accelerator facility to energies higher than that available at LEAR. Finally, there have been studies to use antiprotons for medical imaging and therapy [48, 49, 54]; as well as for enhanced nuclear warhead fission.

To demonstrate this robustness and the feasibility of transporting antimatter, electrons suspended in the same hyperbolic Penning trap used in this work were

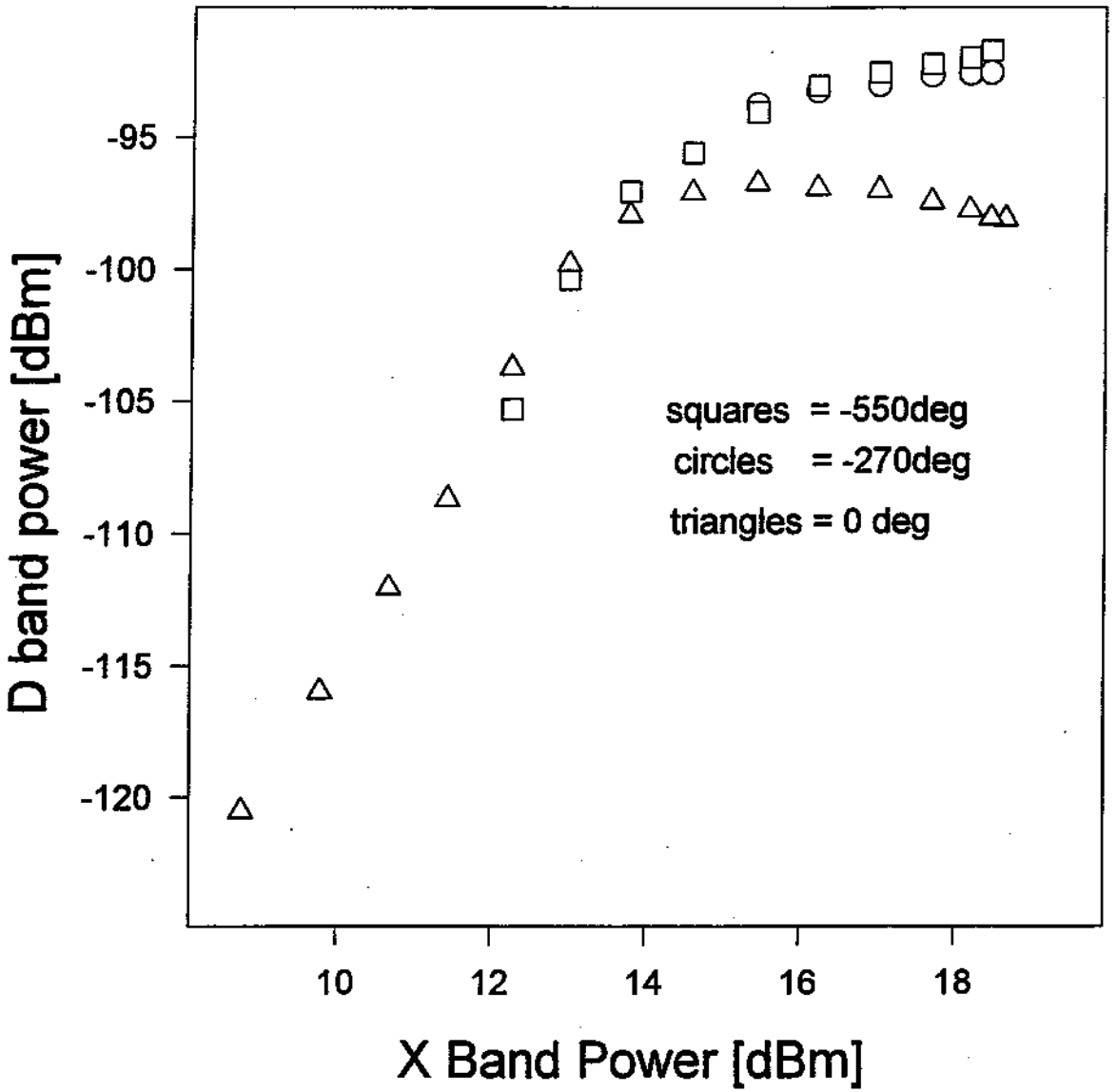

Figure 2.22: Conversion efficiency of X band to D band radiation. The different symbols correspond to positions of the tuning stub. The power is maximized at -550 degrees.

transported five thousand kilometers across the continental United States in the back of a tractor-trailer. This trip is a demonstration that antimatter can be transported over similar long distances. The Penning trap apparatus is very similar to that used to trap antiprotons from LEAR. For a portable trap, a high vacuum is desirable for low loss due to collisions. Also, a high field is necessary for containment of high numbers of particles. With these points in mind, it is natural to use a superconducting solenoid and a cryogenic vacuum. For the portable version of the Penning trap, two ordinary 9 Volt radio batteries provided the trapping potential. The solenoid was energized to about 80 percent (4.7 Tesla) of the full field, and shimmed to a homogeneity of 25 pbb/cm^2. Approximately 6×10^4 electrons were loaded into the trap 51 hours before hoisting the apparatus into the 15 meter long trailer bed. During each of 23 stops the electron number was monitored by a Hewlett-Packard Spectrum Analyzer (Model 8593A). The electron signal was a 'dip' (as discussed in the section on detection electronics) in the liquid helium noise resonance [90]. The number could easily be determined to within 10 percent. A diesel generator was started at each stop to power the detection electronics. During transport, no power (other than the two 9 Volt batteries) was necessary. The trip of 4984 km took a total of 3.68 days with no loss of electrons within measurement precision except for one unfortunate and avoidable incident in Nebraska.

The electrons were lost during a stop at Grand Island, Nebraska because of an ice blockage in the cryostat. The transport path went from Martinez, CA (near sea level), across the Sierra Nevada mountains at Donner Pass, (elevation 2203 meters), across the Rocky mountains near Laramie, Wyoming (elevation 2179 meters), and then across the Plains. These elevation changes caused changes in the liquid helium temperature and thus boiloff. As the boiloff decreased dramatically, moisture crept back through the exhaust tubes and formed an ice blockage in the helium dewar for the superconducting solenoid and in the dewar for the Penning trap. These were unplugged in Echo Reservoir, Utah by inserting the helium transfer tube into the dewar and by flowing helium gas across the ice. The exhaust tubes were extended

in hopes of reducing the backflow. The Penning trap dewar was again plugged when crossing the Rocky mountains. While stopped at Grand Island, Nebraska the Penning trap dewar was warmed up (with loss of the cryogenic vacuum) during an attempt to unplug the ice. While still stopped, the dewar was recooled and another cloud of electrons was loaded into the trap. The remaining 2500 km into Cambridge, Massachusetts went without incident. This ice blockage could be easily avoided in the future with a pressure check valve on the exhaust tubes.

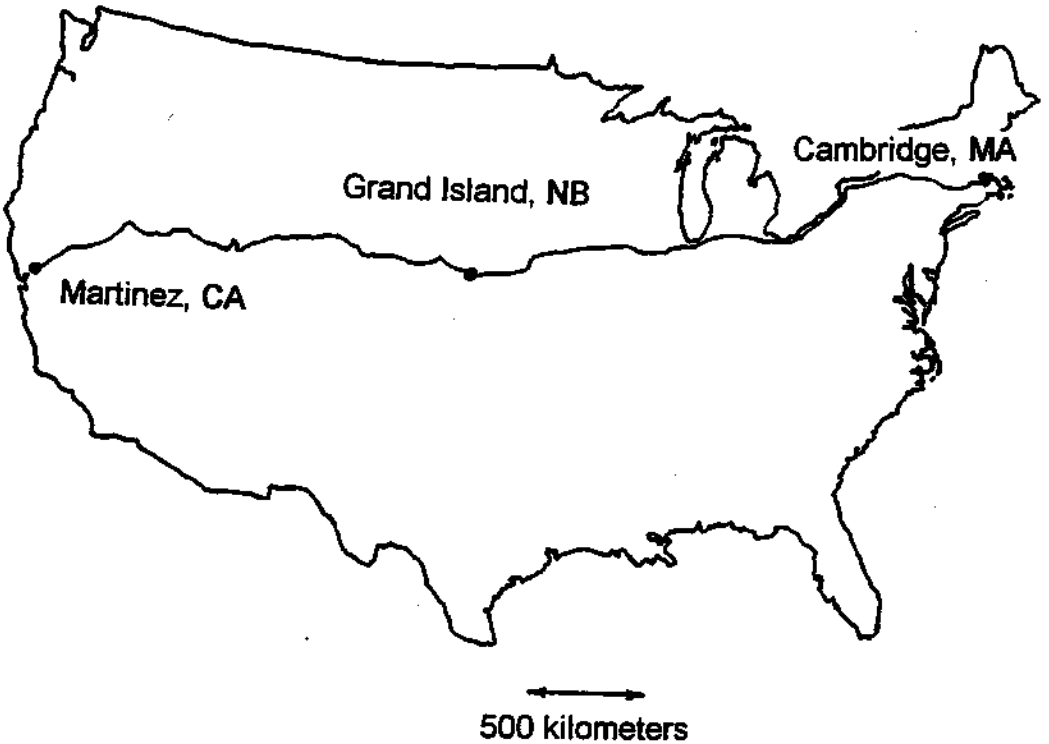

Figure 2.23: Path of electrons transported across the United States.